CHALMERS
UNIVERSITY OF TECHNOLOGY

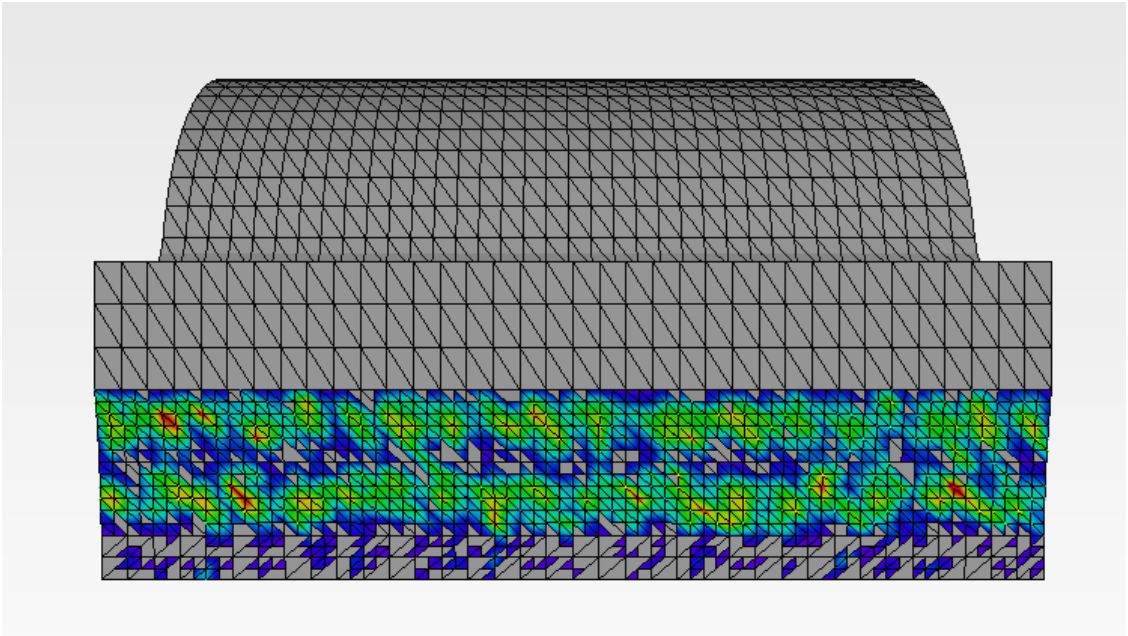

Polygonal contact model for magnetic track brake simulations

Utilization of the Polygonal contact model within SIMPACK for simulations of magnetic track brakes

Master's thesis in Mobility Engineering

Jakub Červenka

DEPARTMENT OF MECHANICS AND MARITIME SCIENCES
CHALMERS UNIVERSITY OF TECHNOLOGY
Gothenburg, Sweden 2025
www.chalmers.se

Master's Thesis in Mobility Engineering

Polygonal contact model for magnetic track brake simulations

Utilization of the Polygonal contact model within SIMPACK for simulations of magnetic track brakes

Jakub Červenka

CHALMERS
UNIVERSITY OF TECHNOLOGY

Department of Mechanics and Maritime Sciences
Division of Dynamics
Chalmers University of Technology
Gothenburg, Sweden 2025

Polygonal contact model for magnetic track brake simulations
Utilization of the Polygonal contact model within SIMPACK for simulations of magnetic track brakes

Jakub Červenka

Supervisor: Emin Kocbay, Christian Doppler Laboratory
Supervisor: Bernhard Ebner, Christian Doppler Laboratory
Supervisor: Johannes Edelmann, Christian Doppler Laboratory
Examiner: Björn Pålsson, Department of Mechanics and Maritime Sciences

Master's Thesis 2025
Department of Mechanics and Maritime Sciences
Division of Dynamics
Chalmers University of Technology
SE-412 96 Gothenburg
Sweden
Telephone +46 31 772 1000

Cover: Contact force distribution on the bottom of a brake shoe

Typeset in LaTeX
Gothenburg, Sweden 2025

Polygonal Contact Model for magnetic track brake simulations
Utilization of the Polygonal Contact Model within SIMPACK for simulations of magnetic track brakes
Jakub Červenka
Division of Dynamics
Department of Mechanics and Maritime Sciences
Chalmers University of Technology

Abstract

This thesis examines the applicability of the Polygonal Contact Model (PCM) for the simulation of contact between the magnetic track brake and the rail. Since improved braking performance is the key for further optimization of the railway system while maintaining high safety standards, accurate and efficient contact modeling approaches are essential. The aim of this study is to evaluate the accuracy of the Polygonal Contact Model implementation in the software Simpack 2025x.1 for the magnetic track brake application. Two scenarios are examined in this thesis. Results of a paraboloid indenter being pressed onto an elastic halfspace are compared to an analytical solution for this problem. The impact of PCM using elastic bodies is also studied on this case. This thesis also describes the preprocessing in Abaqus necessary in order to successfully implement the elastic extension PCM. The viability of use for the railway application is further judged by simulating a new and a worn brake shoe being pressed onto a straight rail.

Keywords: Polygonal Contact Model, Magnetic track brake, Contact modelling, Pole shoe, Simpack, Elastic extension PCM, Abaqus

Acknowledgements

I would like to thank Emin Kocbay, Bernhard Ebner and Johannes Edelmann from the Christian Doppler Laboratory for Enhanced Braking Behaviour of Railway Vehicles for the continuous support, valuable insight and the opportunity to carry out my thesis under their supervision.

Furthermore, I would like to thank Eray Arslan from the institute of Mechanics and Mechatronics of TU Wien and my examiner Björn Pålsson from Chalmers Department of Mechanics and Maritime Sciences for the technical support they have provided during the thesis.

At last, I would like to thank the Chalmers University of Technology and all professors from my courses for providing me with exceptional education, knowledge and experience.

Jakub Červenka, Vienna, June 2025

List of Acronyms

Below is the list of acronyms that have been used throughout this thesis listed in alphabetical order:

BC	Boundary condition
CAD	Computer Aided Design
DOF	Degree of freedom
FEA	Finite element analysis
MBS	Multibody simulations
PCM	Polygonal Contact Model
UIC	International Union of Railways

Nomenclature

Below is the nomenclature of indices, parameters, and units that have been used throughout this thesis.

Indices

k	Index for k-th element
l	Index for layer
n	Index for normal direction
$_{1,2,3}$	Index for body

Parameters

h, b	Foundation layer thickness
A	Area
K	Elastic modulus
E	Young's modulus
E^*	Modified Young's modulus
v	Poisson's ratio
c	Contact layer stiffness
p	Pressure
F	Force
u	Normal penetration
f	Function
r	Distance from the centre of the paraboloid
R	Radius of the sphere describing the paraboloid shape
a	Contact radius
d	Indentation

x, z, y	Coordinates in Cartezian system
α	Rotation around x
β	Rotation around y
γ	Rotation around z
g	Gravitational acceleration
μ	Coefficient of friction

Units

m	meter
cm	centimeter
mm	milimeter
N	newton
kN	kilonewton
s	second
min	minute
h	hour
Pa	pascal
kPa	kilopascal
MPa	megapascal
GPa	gigapascal
Hz	Hertz

Contents

List of Figures

List of Tables

1
Introduction

This master thesis focuses on the utilization of the Polygonal Contact Model (PCM) within the railway industry, specifically the viability of its use for the simulation of contact between magnetic track brake and rail. Comparison of results generated by PCM with an analytical solution by Hertz for a case of a paraboloid indenter is done in order to evaluate the accuracy of the force distribution within the contact patch. The applicability in the case of the magnetic track brake is evaluated based on the results of a worn and unworn brake shoe sliding along a straight rail. The implementation of PCM in the commercial MBS code Simpack is used in this thesis.

1.1 Background

The recent years have introduced many new challenges into the railway industry. One of these challenges is the ability to optimize track usage, in other words run more trains, faster and with a higher payload. Improved braking performance, especially under emergency circumstances, would make this achievable. The magnetic track brake is a common solution for emergency scenarios, especially for passenger vehicles where safety is prioritized. Knowing the characteristics of the contact between the brake and the rail is key in order to further develop this brake. An effective way of examining the contact under various conditions is the use of simulations. [1]

There are many different contact models available, that could be used in such simulations. The most capable by far is the finite element analysis [6]. This method is however very computationally expensive. The use of PCM could bring down the computational effort significantly, given the accuracy is sufficient.

1.2 Purpose & Objectives

The purpose of this thesis is to address the viability of PCM simulations for the given magnetic track brake scenario. By comparing PCM results with analytical solutions and simulating the contact of the magnetic track brake on a straight piece of rail, the feasibility of the model will be evaluated. The following objectives were set in order to fulfill the purpose of the thesis:

- Compare the PCM using rigid bodies to an analytical solution of a paraboloid indenter
- Compare the elastic extension PCM to an analytical solution of a paraboloid indenter

- Evaluate PCM results simulating an unworn pole shoe sliding on a straight rail
- Evaluate PCM results simulating a worn pole shoe sliding on a straight rail

1.3 Scope & Limitations

This thesis focuses on the capabilities of the Polygonal Contact Model within Simpack. A scenario of a paraboloid indenter being pressed onto a halfspace is studied and compared to an analytical solution. Furthermore, performance of the PCM is evaluated simulating contact between the magnetic track brake and a straight piece of rail.

The simulations carried out for the purposes of this thesis used the Simpack 2025x.1 version. As of writing this thesis, the newest version of PCM described in [7] has not been implemented into the Simpack software.

1.4 Disposition

This thesis is structured into 4 main chapters. Chapter 2 introduces the fundamental concepts used in the thesis. Chapter 3 provides a detailed overview of the methodology employed in the simulations, from model preparation to post processing. Chapter 4 presents and evaluates the results of the simulations, while chapter 5 summarizes the main outcomes of the thesis.

2
Technical background

This chapter covers the basic concepts relevant to this master thesis. Section 2.1 provides an overview of the magnetic track brake system. Section 2.2 covers the fundamental principles of the Polygonal Contact Model.

2.1 Magnetic track brake

The magnetic track brake is a specialized brake designed to assist other brake systems. Unlike traditional concepts, it does not utilize the wheel-rail contact, but rather creates a new friction surface between the rail and the vehicle, which is used for the transfer of braking forces. Construction of a magnetic track brake magnet is described in figure 2.1.

Another difference is that the braking force is independent of the weight of the train, but is instead dependent on the magnetic field interacting with the rail. This brake is mostly used in emergency cases, when the available adhesion in the wheel-rail contact is not sufficient. These circumstances usually occur with bad weather conditions when the rail is wet, icy or covered in leaves. [1]

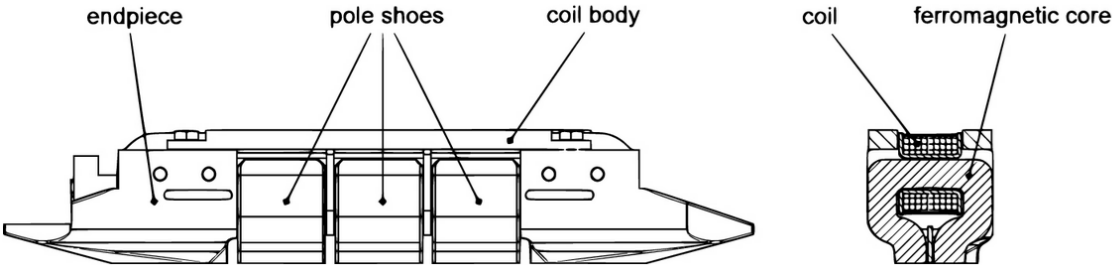

Figure 2.1: Braking magnet with three pole shoes, from [10]

A benefit of the magnetic track brake is that it also cleans the rail surface. In doing so, it improves the available adhesion for the wheel-rail contact. According to studies done by SJ, the use of magnetic track brakes on all bogies can improve the deceleration by $0.3 - 0.4$ m/s^2. [1]

The component that interacts with the rail is the pole shoe. It is usually made out of cast iron or steel. As can be seen from figure 2.2, the contacting surface at the bottom of a new pole shoe is completely flat. This profile changes with the use

of the magnetic track brake and wears off in order to create a shape similar to the shape of the rail head. [1] [9]

Figure 2.2: Geometry of the pole shoe - front

2.2 Polygonal contact model

The Polygonal contact model (PCM) is a method for contact evaluation of complicated geometries. It is based on discretization of the geometry surfaces into polygons and utilization of Winkler's elastic foundation model in order to calculate the contact forces. This method was presented in the early 2000s and has since established itself as a suitable model for multibody dynamics simulations. [6] [7]

The discretization of the body brings many benefits over simpler contact point approximation methods, which utilize geometrical shapes with known analytical solutions. It allows for multiple contact points and it is much more efficient and accurate at modelling complex surfaces. Since it utilizes discretization, it can also be easily combined with existing 3D models or scans. Although the finite element analysis (FEA) still remains the most accurate and powerful tool for contact analysis, it is much more computationally demanding making it cumbersome to use in the case of three dimensional multibody simulations with dynamic behavior. [6]

There are two main aspects to the PCM. The next subsections will take a closer look at how the PCM detects the contact region and how the contact forces are calculated.

2.2.1 Contact detection

There are multiple options on how to evaluate collisions between two bodies. These are mostly based on techniques used in the virtual reality and computer graphics. This section will only describe the method used by the original version of the PCM. This contact detection method utilizes bounding volumes around the two bodies. A contact occurs if there is penetration between the two bounding volumes. Since checking each individual node for contact would be very computationally inefficient, a hierarchical approach is presented. Instead of evaluating every node, the bodies are firstly represented by rough shapes which are easy to evaluate. If a collision is detected, the bodies are further discretised into smaller and more refined shapes. This is repeated until the final tessallation is reached. Figure 2.3 explains the principle behind this approach. For more detail on the contact detection please see [6] [14].

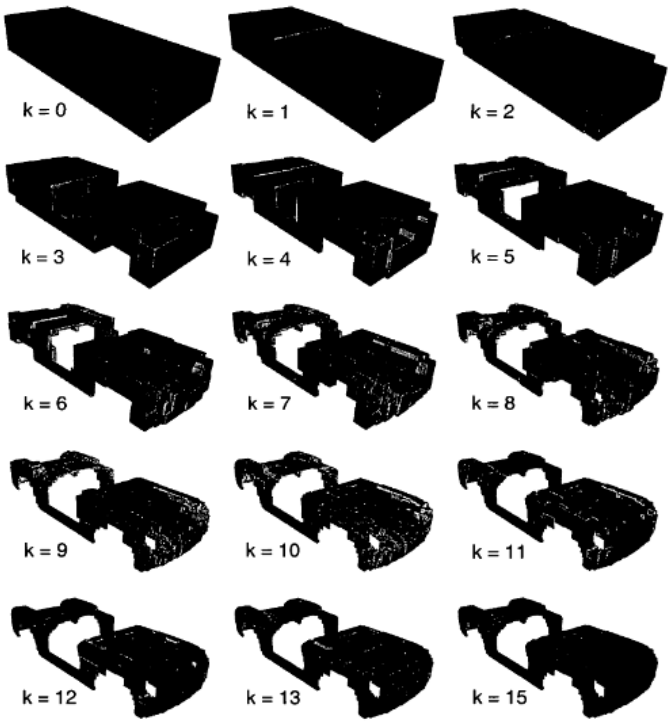

Figure 2.3: Several levels of boundary volume hierarchy, from [5]

2.2.2 Contact force calculation

The PCM utilises the elastic foundation model [8]. The geometry is essentially covered in a layer of springs which are used to determine the contact force, as can be seen in figure 2.4.

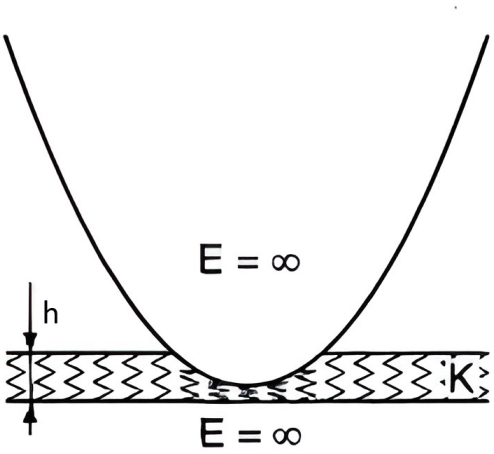

Figure 2.4: Example of an elastic foundation layer, from [5]

The stiffness of Winkler's elastic foundation layer is dependent on the layer thickness h and the elastic modulus K, which can be calculated using material parameters Young's modulus E and Poisson's ratio v under the assumption of thin, linear-elastic layers [13]. The following relation is used in order to determine the elastic modulus K of the foundation layer under the assumption that $v < 0.45$:

$$K = E\frac{1-v}{(1+v)(1-2v)} \tag{2.1}$$

The contact layer stiffness c_l can be determined using the following equation:

$$c_l = \frac{K}{h} \tag{2.2}$$

There is no shear stress occurring in the elastic foundation layer since the springs and dampers do not interact between each other. The normal pressure p can be directly derived based on the normal penetration u:

$$p = \frac{K}{h}u \tag{2.3}$$

The resulting normal contact force for each element F_k can be derived as:

$$F_k = c_l A_k u_k \tag{2.4}$$

Equations 2.1 - 2.4 are based on information from [13] and [6].

2.2.3 Elastic extension of PCM

The original PCM was limited to the use of rigid bodies covered in an elastic foundation layer, meaning that the geometry itself kept the original shape and the deformation occurred only in the elastic foundation layer. In order to achieve more

realistic results especially when simulating more compliant materials, an elastic extension of PCM was introduced. Using this extension allows the deformation of geometries themselves based on the forces calculated in the foundation layer. The computational effort is however much higher than with the rigid body simulations. This is caused by the need of recalculating the bounding volumes in each step due to the change of position relative to the reference system and the modified force calculation. [4]

It is also necessary to provide a flexible body input (.fbi) file, which carries the information about the expected deformation of the geometry. The .fbi file is based on a finite element analysis. A more in depth description of this extension is available in [4]. The workflow of implementing the elastic bodies extension in Simpack is described in chapter 3.

3

Methodology

This chapter will focus on the simulation setup of the paraboloid indenter case using both rigid and elastic bodies. Description of the simulation setup for the case of a worn and unworn pole shoes acting on a straight rail are also part of this chapter.

3.1 Paraboloid indenter

In order to examine the capabilities of the polygonal contact model, a case of a paraboloid intender being pressed onto an elastic half-space was selected. The selection of this particular scenario was motivated by the availability of an analytical solution for two linear elastic bodies in contact provided by Hertz [12], and the possibility of further comparison with a contact model developed by Christian Doppler Laboratory for Enhanced Braking Behavior of Railway vehicles [10]. The surface of the paraboloid can be described by the following relation:

$$z(r) = \frac{r^2}{2R} \tag{3.1}$$

where r is the radial distance in the XY plane from the center of the paraboloid and R denotes the radius of the sphere. For our case, value of $R = 50$m was used as it could later be used for comparison with [10]. The cross-sectional cut displaying the curvature of the surface along x axis can be seen in figure 3.1. Source [10] provides the solution to the normal pressure distribution for this particular scenario as the following equation:

$$-p(r) = \frac{-2E^*}{\pi R} sqrt(a^2 - r^2) \quad , r \leq a \tag{3.2}$$

where E^* is the effective Young's modulus and a is the total contact radius. The effective Young's modulus can be calculated using the following relation:

$$\frac{1}{E^*} = \frac{1 - v_1}{E_1} + \frac{1 - v_2}{E_2} \tag{3.3}$$

where E_i is each material's Young's modulus and v_i is each material's Poisson's ratio. Total contact radius a can then be calculated using the following equation:

$$a = \sqrt[3]{(\frac{3F_n R}{4E^*})} \tag{3.4}$$

where F_n is the applied normal force. The maximum indentation can be established using the following relation:

$$d = \frac{a^2}{R} \tag{3.5}$$

Equation 3.1 is based on information from source [12] and equations 3.2 - 3.5 are based on information from source [10].

To achieve meaningful results both for the comparison with [10] and for observing the behavior of the polygonal contact model with material parameters used in rails and brake shoes, two scenarios with different E were studied. Simulations for both the softer, rubber-like material ($E = 3.5$MPa, $v = 0.3$) and the stiffer, steel material ($E = 210$GPa, $v = 0.3$) were carried out. Please note that the same material was used for both bodies, meaning $E = E_1 = E_2$ and $v = v_1 = v_2$.

3.1.1 Geometry definition in CAD software

The characteristic shape of the paraboloid in figure 3.1 was created using a curve based on the following equation:

$$z = \frac{x^2}{2R} \tag{3.6}$$

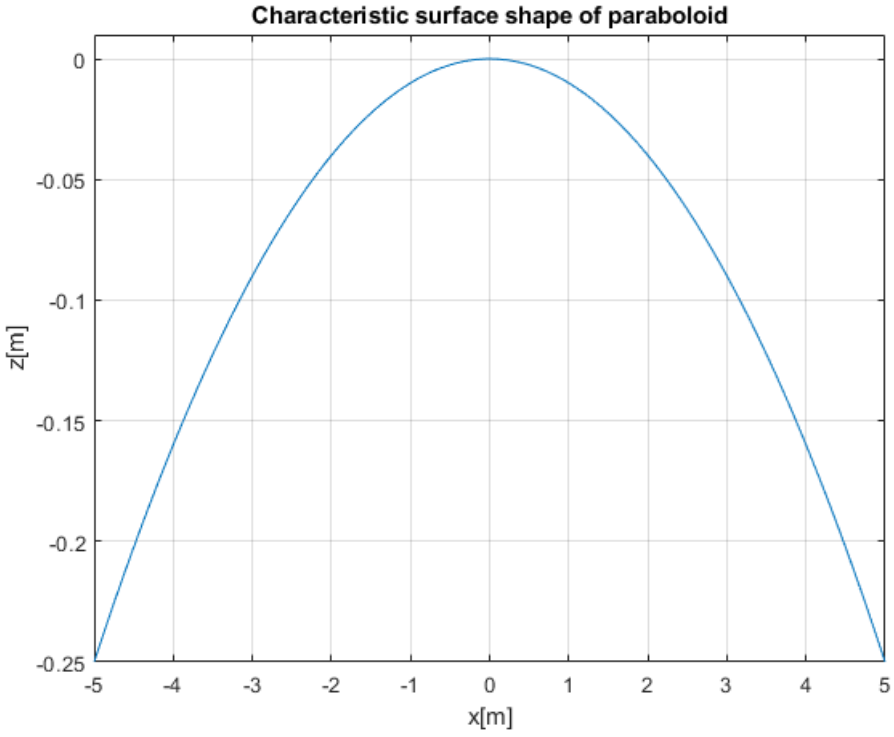

Figure 3.1: Shape of the paraboloic surface

The values of x were changed between simulations in order to provide the most efficient computational times. The values were based on the calculated contact radius for the specific scenario. For the simulations with the softer material, the range of values was set to $x = [0, 2]$m and for the stiffer material, the range was set to $x = [0, 0.05]$m. The curve was then closed off and revolved around the z axis. The final geometry can be seen in figure 3.2.

Figure 3.2: Geometry of paraboloid in software Creo

The geometry of the half-space was simplified to a square prism. The sides of the square were chosen accordingly to the contact radius to be $a = 2$m for the more elastic case and $a = 0.12$m for the stiffer case. These values were chosen based on the calculated contact radius using equation 3.4, with an additional buffer to ensure the results are not affected by insufficient body size . The square was then extruded in order to get the square prism. The thickness of the extrusion was set to 0.5m for the softer material scenario and 0.01m for the stiffer material case. These extrusions are sufficiently thick compared to the expected maximum indentation depths and should not impact the results. The final geometry for the stiffer scenario can be seen in figure 3.3.

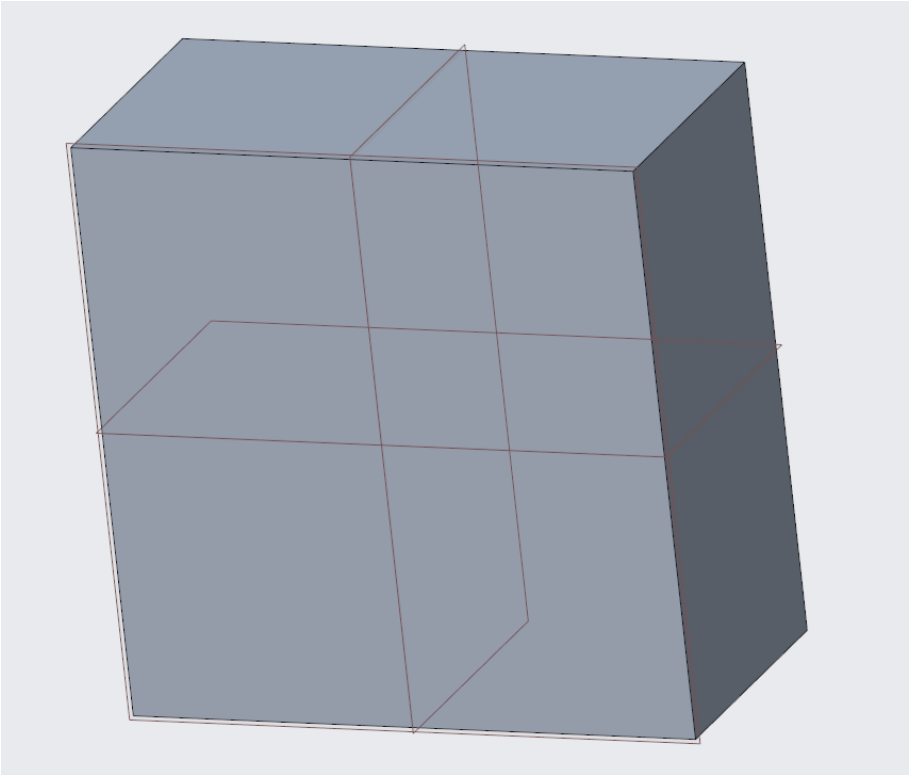

Figure 3.3: Geometry of half-space in software Creo

The setup of the simulations in Simpack requires a different approach for the PCM using only rigid bodies and the PCM using the elastic extension. The workflow for the rigid only PCM is described in sections 3.1.2 and 3.1.3, and the workflow for the elastic extension PCM is described in sections 3.1.4 and 3.1.5.

3.1.2 Abaqus model preparation - rigid body

When using only the rigid bodies in PCM, the only step conducted outside of the Simpack consists of meshing the geometries. The geometries were meshed according to the simulation using tetrahydral C3D10 elements. An example of a meshed paraboloid is shown in figure 3.4. The geometry was then exported as a .obj file. The mesh seed for each simulation is documented in chapter 4.

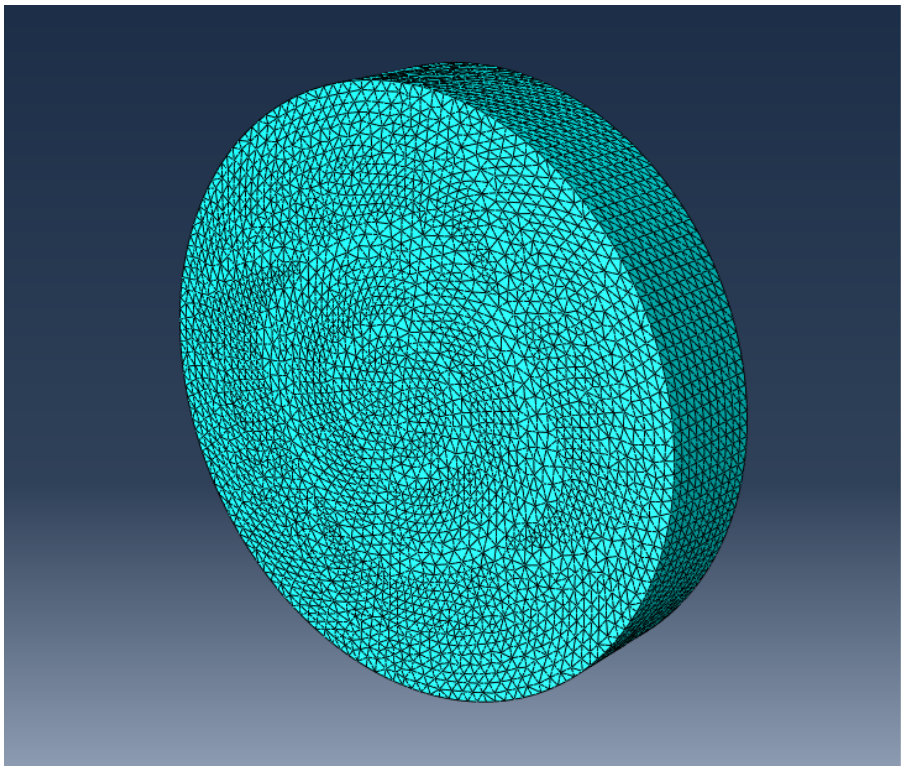

Figure 3.4: Mesh of paraboloid in Abaqus 2024

3.1.3 Simpack simulation setup - rigid body

The simulation setup shown in figure 3.5 consists of 2 bodies: the paraboloid and the simplified half-space. Both bodies are placed in the original coordinate system using joints. The joint type for the half-space is of type 0: 0 degrees of freedom, whereas the joint for the paraboloid is of type 6: Prismatic z. This allows the paraboloid to be pressed onto the other geometry. The geometry types are set to type 39: `CAD Interface` and the .obj exports from Abaqus are imported. It is important to note, that Simpack further refines the .obj import. A mesh with a seed of 0.1m in Abaqus will be refined to a mesh with approximately half the seed (0.05m) in Simpack. There are two force elements active in the simulation. The force element acting as the pressing force on the Paraboloid is of type 5: `Spring-Damper Parallel Cmp`. The force is applied between the two reference markers of each geometry. The only non-zero parameter is the nominal force in z, which contains the value of force applied to the paraboloid. The other force element active in the simulation is of type 199: Polygonal Contact (PCM). This force element handles the contact calculation. Only the most important settings of this force element will be covered in this section. The full settings are available in appendix A.

The two most important settings for the paraboloid scenario are the foundation layer thickness settings and the selection of master and slave geometry. The surface with the finer discretization should be selected as the master surface in order to get the best results [3]. In our case, combination Half-space/Paraboloid was chosen as the Master/Slave. There are three different settings related to the foundation layer

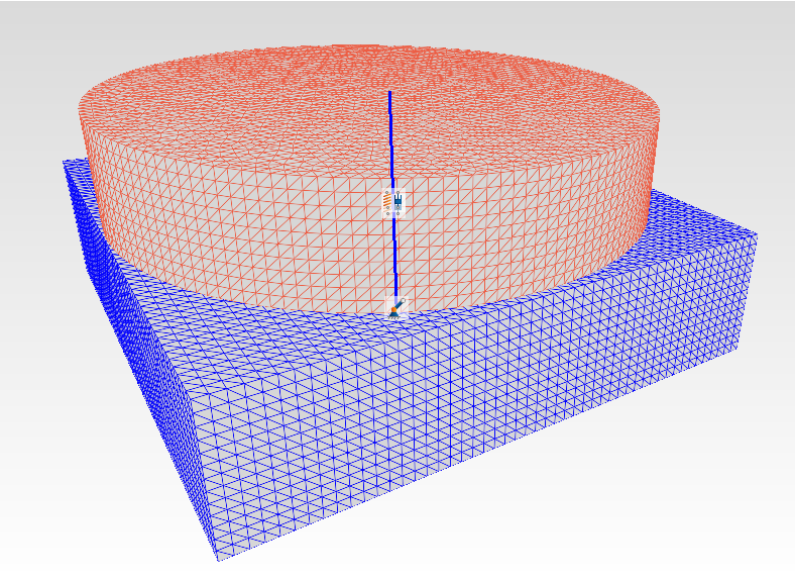

Figure 3.5: Simulation setup in Simpack

thickness. Young's modulus and Poisson's ratio are based on the material parameters. Source [12] suggests the use of equation 3.7 for axi-symmetric cases in order to achieve the results comparable to the Hertzian solution.

$$h = \frac{Ka}{1.7E^*} \tag{3.7}$$

The suggested layer thickness using a reference force of $F_n = 4860\text{N}$ was calculated to be $h = 0.657\text{m}$ for $E^* = 1.923\text{MPa}$, and $h = 0.0168\text{m}$ for $E^* = 115.38\text{GPa}$. The use of effective Young's modulus E^* implies, that the foundation layer of the slave geometry will have $h \to 0$ while the master will use the calculated value. This will result in the same behavior as if each foundation layer would have used the non-modified E and both layers would use an according h. This approach was utilized in the rigid body paraboloid simulations.

It is important to note, that the calculation 3.7 considers h as a variable across the foundation layer, whereas Simpack only allows a constant h to be selected for the PCM. The value of a is not necessarily constant across the whole contact surface, especially for complex geometries. This introduces errors and necessitates comparing the results with an analytical solution or selecting the foundation layer thickness very carefully. [12]

Since we are only interested in the quasi-static behavior, the equilibrium is first calculated in order to minimize computational effort. The solver settings for the calculation of equilibrium are available in appendix A. After the model has been put into equilibrium, a time integration simulation is carried out. Source [3] suggest the use of SODASRT2 integration method due to accuracy and computational efficiency. The output of the time integration provides the solution of the contact problem. The studies carried out using the PCM with only rigid bodies can be found in table 3.1.

Table 3.1: Overview of studies done using rigid body PCM

$E*$	**Study**
1.923 MPa	Mesh convergence
1.923 MPa	Influence of h
1.923 MPa	Influence of F_n
115.38 GPa	Mesh convergence
115.38 GPa	Influence of h
115.38 GPa	Influence of F_n

3.1.4 Abaqus model preparation - elastic extension

The use of the elastic extension of PCM requires prior simulations in order to generate a flexible body input file (.fbi), which is necessary for such simulations in Simpack. It is important to check the compatibility between the versions of Abaqus and Simpack, since this may lead to bugs. The generation of a .fbi file begins with meshing, which is done in a similar manner as in section 3.1.2. After the mesh has been generated, it is necessary to specify the material parameters (density and elastic properties), create and assign a section. A coupling has to be established between a control point and the controlled surface. The control point, also called the master node, is later used to connect the body within Simpack and a marker is generated in the location of this node. There are two options for this coupling. In the case of kinematic coupling, the controlled surface performs a rigid body motion based on the motion of the control point. When using distributed coupling, the input received by the master node is distributed across the controlled surface. For more information regarding types of couplings refer to [2]. For our specific case, kinematic coupling was chosen between a master node and the surface, which will be fixed during the frequency analysis step.

In order to establish expected deformation, a modal analysis is required. This is done via the frequency analysis step. In our case, the boundary condition selected for this step locks all degrees of freedom of the master node, and due to the coupling also the controlled surface. The settings of the modal analysis are shown in figure 3.6. Two types of boundary conditions were examined. The first boundary condition (BC-1) assumed that only the opposite surface to the contact surface has all the degrees of freedom locked. The second boundary condition (BC-2) assumes that both the half-space and the paraboloid indenter have all of the faces which do not come in contact with the other bodies fixed. For figures of the boundary conditions please refer to the appendix A.

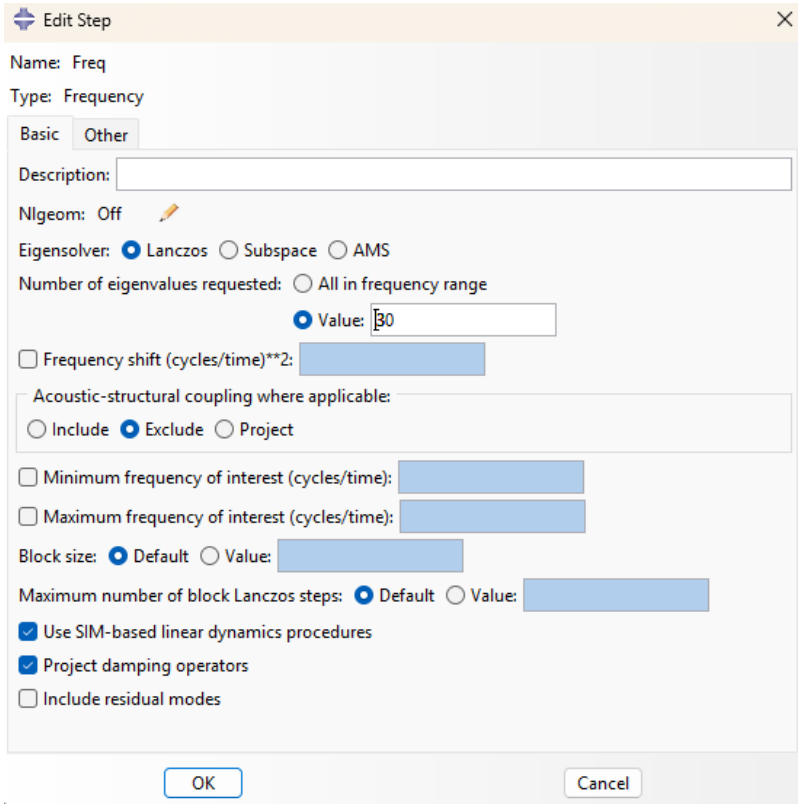

Figure 3.6: Settings of the modal analysis in Abaqus

The last step in the generation of the .fbi file is the substructure generation. In our case, the boundary condition selected for this step retains all of the degrees of freedom of the master node. The configuration used for this step is shown below.

```
** STEP: Substructure
*Step, name=Substructure, nlgeom=NO
*Substructure Generate, overwrite, type=Z100, recovery matrix=YES,
mass matrix=YES
*Select Eigenmodes, generate
1, 30, 1
*Flexible Body, type=SIMPACK
*Damping Controls, structural=COMBINED, viscous=COMBINED
*Retained Nodal Dofs
_PickedSet22, 1, 6
*End Step
```

3.1.5 Simpack simulation setup - elastic extension

The simulation in Simpack consists of two bodies of type `Linear flexible`. After selecting the flexible body input file, the geometry is automatically imported. Using the linear flexible bodies requires the generation of markers in the position of the master nodes in order to connect the geometry to the coordinate system. Markers

generated were of the type `At node`. At last, the eigenmodes have to be activated for the body in order to account for the deformation. There is also the possibility of disabling inertia relief modes. The formulation of the force elements was done in a similar manner as in section 3.1.3. The only difference was in the parametrization of the elastic boundary layer, since it was not possible to use the simplification mentioned in section 3.1.3. The layer thickness was approximated at first and fine tuned through iteration. The same thickness was used for both bodies. Due to convergence errors and much higher computational effort, the step of finding the equilibrium was skipped. In order to reach the quasi-static point quickly, the simulation used a small coefficient of restitution 10^{-5}. The time integration simulation was ran for 4 seconds with a sampling rate of 300Hz. All possible settings options can be found in [3].

The following studies were done for both of the previously mentioned boundary conditions using the elastic extension PCM:

Table 3.2: Overview of studies done using elastic extension PCM

E^*	**Study**
1.923 MPa	Influence of activated modes
1.923 MPa	Comparison with rigid results
115.38 GPa	Influence of activated modes
115.38 GPa	Comparison with rigid results

3.1.6 Postprocessing in Matlab

The output of the PCM force element from Simpack does not contain the normal pressure explicitly, thus needs to be calculated based on the normal force and the nodal area of each node. The following formula was used to calculate the normal pressure for each node:

$$p_k = F_k / A_k \tag{3.8}$$

3.2 Pole shoe slid on a straight rail

Two different geometries of pole shoes acting on a rail head were examined. Simulations using an unworn pole shoe and a worn pole shoe were carried out. Rail profile UIC60 was used in the simulations. Only rigid bodies were used in these simulations due the small impact of the elastic extension PCM on stiff bodies.

Meshing of the bodies was done in a similar manner as in section 3.1.2. The mesh was refined only near the expected contact region in order to keep the size of the files small. Mesh quality for each simulation is described in section 3.2.1 and 3.2.2 respectively. Due to the expected symmetry in the contact and in order to minimize the simulation run time, only half of the pole shoe was used in the simulations.

In order to fully understand the expected forces and the movement of the pole shoe from the simulation setup in figure 3.7, a master thesis [11] focusing on the

finite element simulations of such brakes was studied. The results of the thesis show, that the mounting solution for the pole shoe which connects it to the rest of the magnetic track brake causes a forward tilting moment, which in turn moves the forces to the front of the pole shoe in the direction of travel.

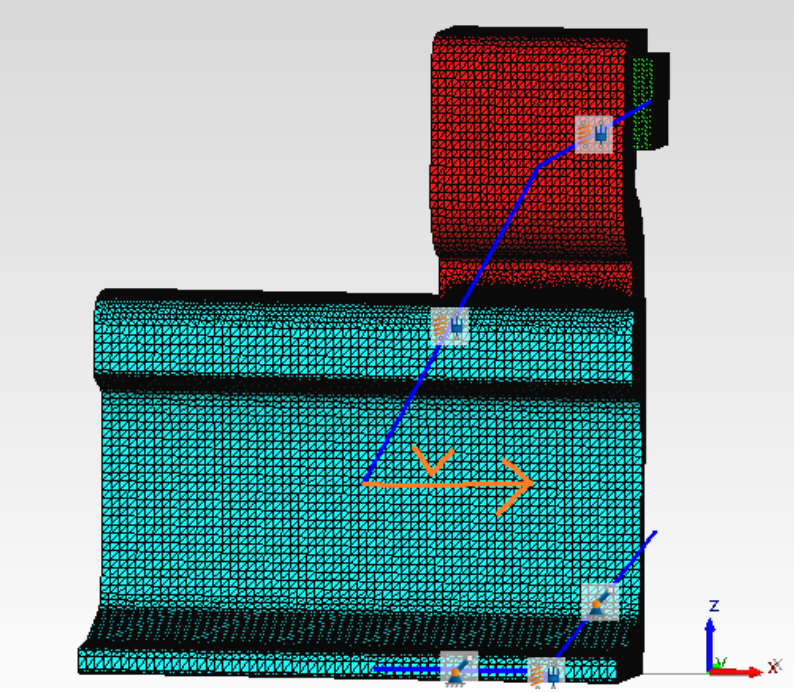

Figure 3.7: 3D model in Simpack – Unworn pole shoe

3.2.1 Simulation setup - Unworn pole shoe

The setup of the simulation examining the unworn pole shoe being pressed onto the rail head surface consists of three bodies. The rail is connected to the system using the joint type `27:Single Axis Constant Velocity`. The pole shoe is placed in the system using a joint of type `25:User Defined`, which locks the movement along the Y-axis and the rotations α and γ. The simplified mounting mechanism, for simplicity called push block, is placed into the system using a 0 DOF joint. The push block was added to the simulation in order to get the tilting effect mentioned in section 3.2.1. The geometry of the pole shoe can be seen in figure 2.2. A mesh seed of approximately 0.3mm was used in the contact region. The settings of the joints as well as the pictures of other geometries used are available in appendix A.

There are two force elements of type `5:Spring-Damper Parallel Cmp`. One simulates the simplified effect of the magnetic attraction and the other one counteracts the effect of mass of the brake shoe. The summary of non-zero parameters used in the element settings is shown in table 3.3. A typical value for the magnetic attraction between one pole shoe and the rail was chosen as 4860 N. Since only half of the model is used, this value was adjusted to 2430 N in order to achieve the same result.

Table 3.3: Overview of force elements of type 5 for unworn pole shoe simulations

Purpose:	Magnetic attraction	Counteract gravity
From Marker:	Centre of coordinate system	Centre of coordinate system
To Marker:	Reference marker - Pole Shoe	Reference marker - Pole Shoe
F_z**:**	2430 N	$m_{poleshoe}g$

The force element `199:Polygonal Contact (PCM)` was used for the evaluation of contact between the rail and the pole shoe in a similar manner as was done in section 3.1.3. The rail geometry was chosen as the master E and the pole shoe geometry was chosen as the slave F. Since we are interested in the quasi-steady sliding of the two surfaces, a small coefficient of restitution of 1e-5 was chosen for both elements. Friction coefficient $\mu = 0.2$ was selected for this simulation. The PCM force element was also used in order to evaluate the contact between the push block and the pole shoe in order to achieve the tilting moment.

Since this problem is not axi-symmetric, a different equation has to be used in order to estimate h. Source [8] suggests the use of equation 3.9 in order to model the compliance of the contact patch accurately.

$$h = \frac{Ka}{0.6E^*} \tag{3.9}$$

The value of contact width a was first guessed and then fine tuned based on the simulation results. Parameters used for the foundation layer are described in table 3.4 and the overview of the model can be seen in figure 3.7.

Table 3.4: Overview of force elements of type 199 for unworn pole shoe simulations

Interaction	$E_1 = E_2$	$v_1 = v_2$	$h_1 = h_2$
Rail – Pole Shoe	210 GPa	0.3	0.004 m
Push Block – Pole Shoe	210 GPa	0.3	0.001 m

Since there are no simulation results using other contact evaluation models for this particular scenario, we are only going to conduct one simulation in order to evaluate the success of generating the tilting moment on the pole shoe. The simulation time was set to 0.5s in order to let the system reach the quasi-static point and a sampling frequency of 4000Hz was used. The simulation was carried out using the SODASRT 2 solver with the absolute tolerance set to 1e-05 and relative tolerance 1e-07.

3.2.2 Simulation setup - Worn pole shoe

The geometry used for the worn pole shoe simulations can be seen in figure 3.8. The wear pattern was created as conforming to the rail surface. The same approach of using only half of the model was selected.

Figure 3.8: Geometry of the worn pole shoe - frontal view

The simulation setup in Simpack for the worn pole shoe case is fairly similar to the one described in section 3.2.1. The joints and the force elements of type `5:Spring-Damper Parallel Cmp` are exactly the same. The only parameter changed in the settings of the force element `199:Polygonal Contact (PCM)` evaluating contact between the pole shoe and the rail is the foundation layer thickness h. The first simulation was carried out using an estimate value of h. The value $h = 0.0163$ m used for simulations described in table 3.5 was set using the formula 3.9 and the value of a based on the initial simulation. The conformal shape of the pole shoe and rail introduced convergence issues, when we tried to use two force elements `199:Polygonal Contact (PCM)`. Instead of using the PCM to resolve the contact between the push block and pole shoe, the tilting motion was achieved using a kine-

matic constraint between a marker simulating the contact point on the push block and a marker on the pole shoe. The constraint only allows for movement along the Z-axis and the rotation β. It is important to select the marker on the pole shoe as the from marker in the settings of the constraint, since moment is only applied to this marker. Choosing the markers in a different manner would not result in the desired tilting moment. The settings of the kinematic constraint can be found in appendix A and the overview of the model can be seen in figure 3.9. Table 3.5 describes the studies carried out and parameters used in the simulations.

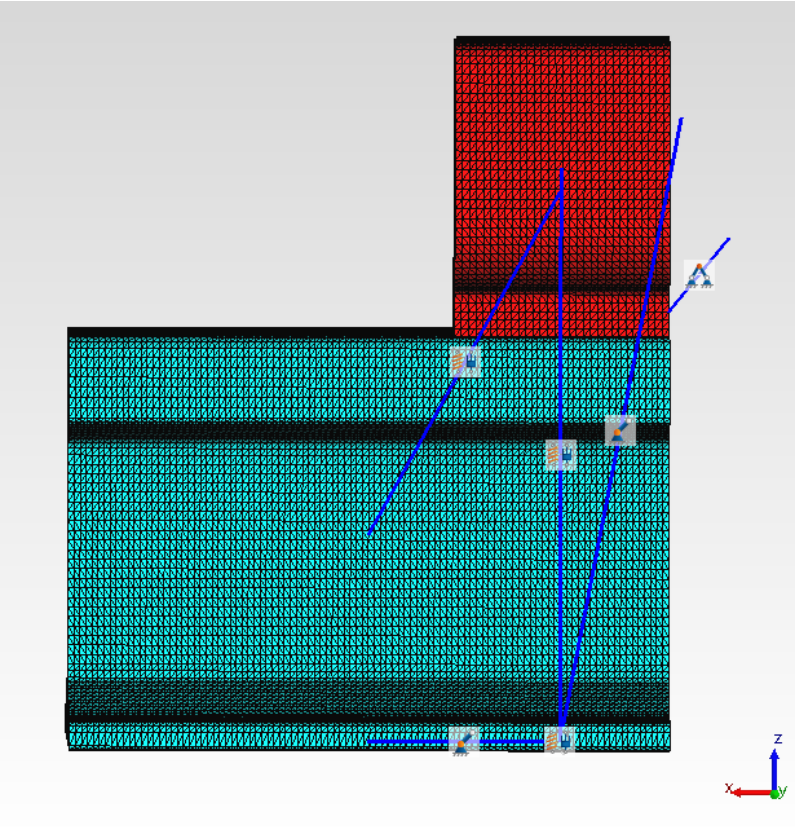

Figure 3.9: 3D model in Simpack – Worn pole shoe

Table 3.5: Overview of studies done using the worn pole shoe

Study	μ	**Mesh seed [mm]**	**Solver**
Mesh convergence	0.2	various	SODASRT 2
Solver comparison	0.2	1 (rail), 1.1 (pole shoe)	various
Impact of μ	various	1 (rail), 1.1 (pole shoe)	SODASRT 2

4

Results

Within this section, results based on the simulations described in section 3 are discussed. In section 4.1, the results for the case of a paraboloid indenter using rigid body PCM are studied and compared to the analytical solution. Section 4.2 studies the impact of the elastic extension PCM on the results and compares them to the rigid body simulations. Sections 4.3 and 4.4 cover the results for the pole shoe being slid on a straight piece of rail.

4.1 Paraboloid indenter - rigid body results

This section covers the results of the simulations mentioned in section 3.1.3. First, a mesh convergence study was conducted in order to mitigate the computational times and provide satisfactory accuracy for the latter simulations.

4.1.1 Mesh convergence study - soft case

The mesh convergence study for the soft case was carried out using the material parameter $E^* = 1.923$MPa and a reference force $F_n = 4860$N. The value of elastic foundation layer thickness $h = 0.657$m used was based on the calculation mentioned in section 3.7. The pressure distribution along the x-axis for each mesh can be seen in figure 4.1 and 4.2. In order to see the impact of the mesh quality on the simulation time, a comparison of the computation times for each seed was conducted. The computational times presented are of simulations measuring a 1 second period using a single core of an AMD Ryzen 5600H processor. The comparison of the computational times can be seen in table 4.1.

Table 4.1: Simulation run time comparison

Seed [cm]	**Run Time [s]**
10	16
7	50
5	192
4	353
3	1278
2.5	2806

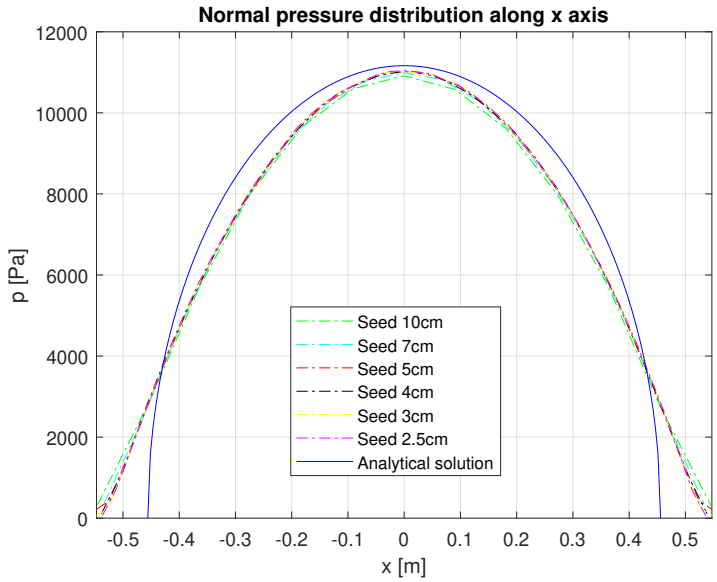

Figure 4.1: Pressure distribution - mesh convergence study (soft case)

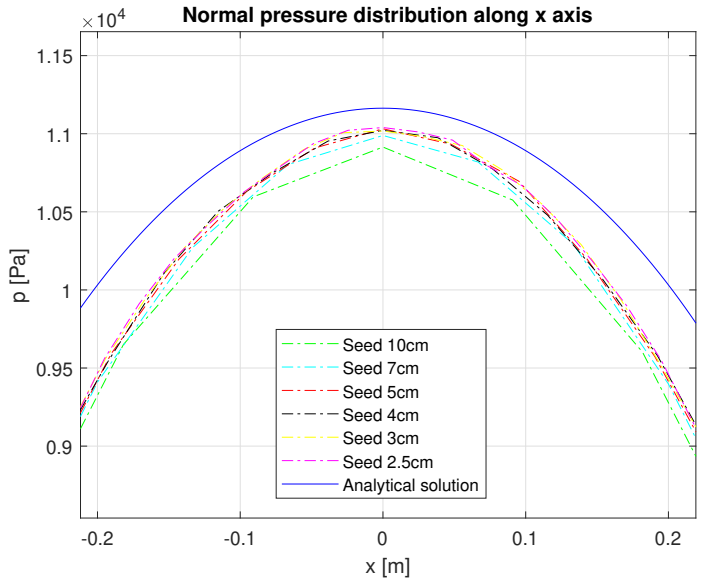

Figure 4.2: Pressure distribution zoomed in - mesh convergence study (soft case)

Based on these results, mesh with a seed of 5cm has been selected for next simulations due to a relatively low computation time, satisfying accuracy and fine enough contact resolution. Please note, that the seed shown in the plots is based on the Simpack simulation, not the geometry generated in Abaqus.

4.1.2 Influence of foundation layer thickness - soft case

After the sufficient mesh quality was established, the influence of the foundation layer thickness on the results was studied. It is important to know the influence of

the foundation layer thickness h in order to estimate possible errors in simulations where the determination of h is not easily doable or can not be verified. The values of h selected for the simulations can be seen in table 4.2. All of the simulations were carried out using the same E^* and F_N as in section 4.1.1.

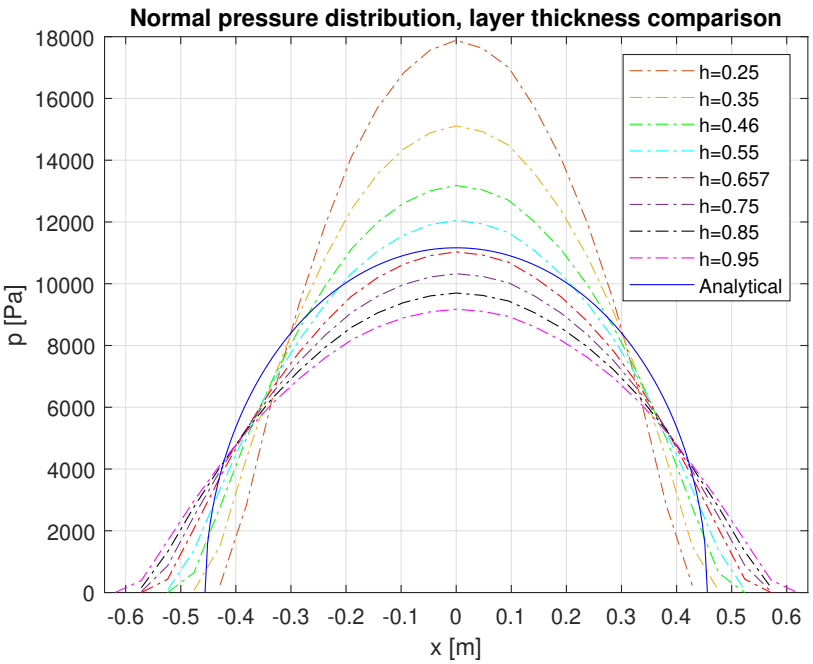

Figure 4.3: Pressure distribution - influence of h (soft case)

The results presented in figure 4.3 are further quantified in the table 4.2. The normalized values are based on the following calculations.

$$h_{norm} = \frac{h}{h_{calculated}} 100 \tag{4.1}$$

$$r_{norm} = \frac{r_{sim}}{r_{analytical}} 100 \tag{4.2}$$

$$p_{norm} = \frac{p_{maxsim}}{p_{maxanalytical}} 100 \tag{4.3}$$

The results presented in table 4.2 indicate that as long as the foundation layer thickness is within 25% of the value calculated according to equation 3.7, the results are fairly accurate. It is important to note that even the simulation result when using the calculated value of h still does not give 100% accurate results. While the value of maximum pressure is very similar to the analytical value of $p_{max} = 11.16$kPa, the contact radius is 25% higher than the analytical solution. This is likely caused by the Winkler foundation layer. The foundation layer is just an approximation of the contact and does not take into account the elastic behavior of the bodies. There is also no deformation outside of the contact region since the individual springs of the foundation layer do not interact with each other.

Table 4.2: Quantified results - influence of h (soft case)

h [m]	h_{norm}	r_{sim} [m]	r_{norm}	p_{maxsim} [kPa]	p_{norm}
0.25	38%	0.43	94%	17.89	160%
0.35	53%	0.48	104%	15.12	135%
0.46	70%	0.52	115%	13.18	118%
0.55	84%	0.52	115%	12.06	108%
0.657	100%	0.57	125%	11.03	99%
0.75	114%	0.57	125%	10.33	92%
0.85	129%	0.57	125%	9.70	87%
0.95	145%	0.62	136%	9.17	82%

4.1.3 Influence of applied force - soft case

Since the force applied between the bodies must not always be constant or the value of the force may have been estimated incorrectly, the influence of using different force values is studied. The simulations were carried out using the values $E^* = 1.923$MPa and $h = 0.657$m. Since the analytical solution changes with the force applied, the plots of the pressure distribution are available in appendix B. Table 4.3 contains quantitative results calculated in the same way as in section 4.1.2.

Table 4.3: Quantified results - influence of F_n (soft case)

F_n [kN]	r_{sim} [m]	r_{norm}	p_{maxsim} [kPa]	$p_{maxanalytical}$ [kPa]	p_{norm}
1	0.38	141%	5.00	6.59	76%
2	0.43	126%	7.08	8.3	85%
3	0.48	123%	8.67	9.50	91%
4	0.52	123%	10.01	10.46	96%
4.86	0.57	125%	11.03	11.16	99%
6	0.57	117%	12.26	11.98	102%
7	0.62	120%	13.24	12.61	105%
8	0.62	115%	14.16	13.18	107%

These results indicate that underestimating the force when calculating the parameters for the simulation has a smaller impact than using a value that may be too high. The overall impact on the errors in contact radius and maximum pressure are quite small.

After studying the behavior of PCM combined with soft material parameters, similar studies were carried out using a stiffer material parameter $E^* = 115$GPa.

4.1.4 Influence of foundation layer thickness - stiff case

Since the mesh quality giving sufficient resolution was already established in section 4.1.1, a mesh providing similar resolution in the contact are was generated. The value of $a = 11.6$mm was calculated using equation 3.4 with the reference force $F_n = 4860$N. In order to achieve a similar resolution a seed of 1.2mm was chosen for

the mesh generation. The foundation layer thickness was set to $h = 0.017$m based on equation 3.7. However, as can be seen in figure 4.4, this value was not correct. This introduced a necessity to establish h by iteration. The comparison of results using different values for h can be seen in figure 4.5 and in table 4.4. The values were calculated in the same manner as in section 4.1.1. Based on these results, the value of $h = 0.07$m was established as the baseline for the latter simulations.

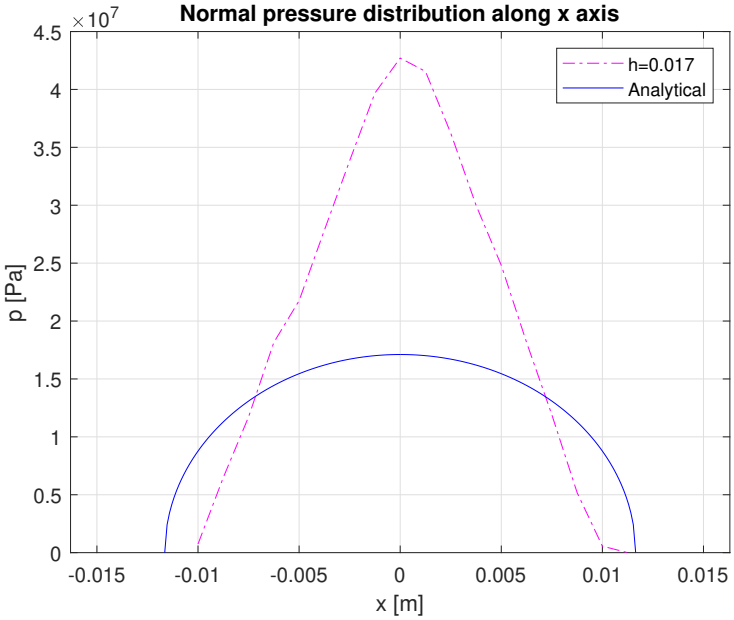

Figure 4.4: Pressure distribution - $h = 0.017$m (stiff case)

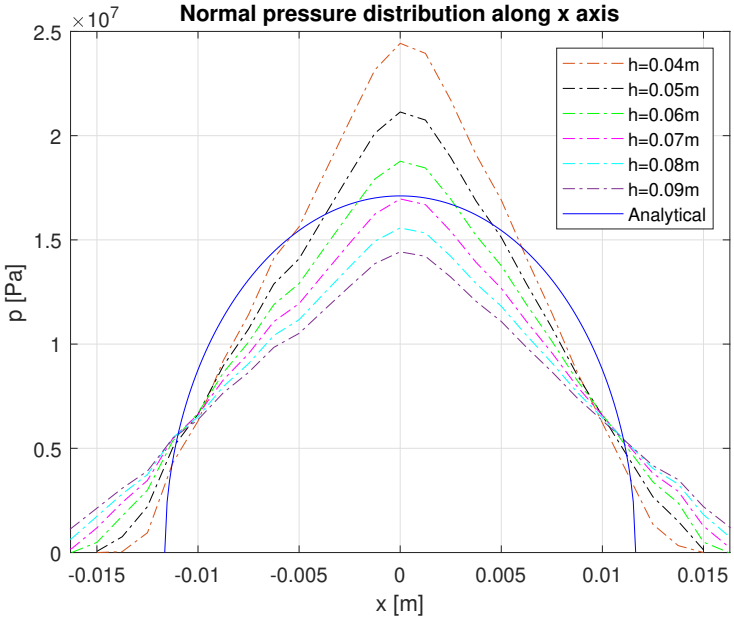

Figure 4.5: Pressure distribution - influence of h (stiff case)

The shape of the pressure distribution however still does not satisfy our requirements

for accuracy, as it does not match the solution by Hertz. For this reason, a mesh convergence study was carried out in order to rule out possible mesh issues. The study confirmed that the mesh quality was sufficient and both finer and coarser meshes did not generate results significantly different. The results of the mesh convergence can be found in appendix B.

Table 4.4: Quantified results - influence of h (stiff case)

h [m]	r_{sim} [mm]	r_{norm}	p_{maxsim} [MPa]	p_{norm}
0.04	15	128%	24.4	143%
0.05	15	128%	21.1	124%
0.06	16.2	140%	18.8	110%
0.07	17.5	150%	17.0	99%
0.08	18.8	161%	15.6	91%
0.09	18.8	161%	14.4	84%

4.1.5 Influence of applied force - stiff case

A similar study as in section 4.1.3 was carried out in order to see the impact of varying the applied force on the results. The summary of the results are available in table 4.5 and the pressure distributions are attached in appendix B.

Table 4.5: Quantified results - influence of F_n (stiff case)

F_n [kN]	r_{sim} [mm]	r_{norm}	p_{maxsim} [MPa]	$p_{analytical}$	p_{norm}
1	10	145%	9.68	10.1	95.9%
2	12.5	144%	12.42	12.72	97.6%
3	15	151%	14.33	14.57	98.3%
4	15	137%	15.85	16.03	98.8%
4.86	17.5	150%	16.97	17.11	99.1%
6	18.75	150%	18.27	18.35	99.5%
7	20	152%	19.28	19.32	99.8%
8	20	145%	20.2	20.2	100%

4.1.6 Behavior of PCM - stiff material

In order to understand what causes the shape of the pressure distribution in figure 4.5, a simulation using a force that would lead to the same deformation as in the soft case was carried out. The force applied to the simulation was $F_n = 8$MN and the layer thickness used was $h = 0.5$m. As can be seen in figure 4.6, the paraboloic shape of the pressure distribution is achieved while still using the stiffer material parameters. Source [7] states the issues of extended computational time, robustness and even complete failures of the PCM in simulations containing conforming contact in combination with high stiffness or low penetration. This was the case with using the material parameter $E^* = 115$GPa in combination with the relatively low force.

The shape of the paraboloid with the chosen parameters is almost completely flat in the contact patch, which possibly causes the shape of the pressure distribution achieved in section 4.1.4.

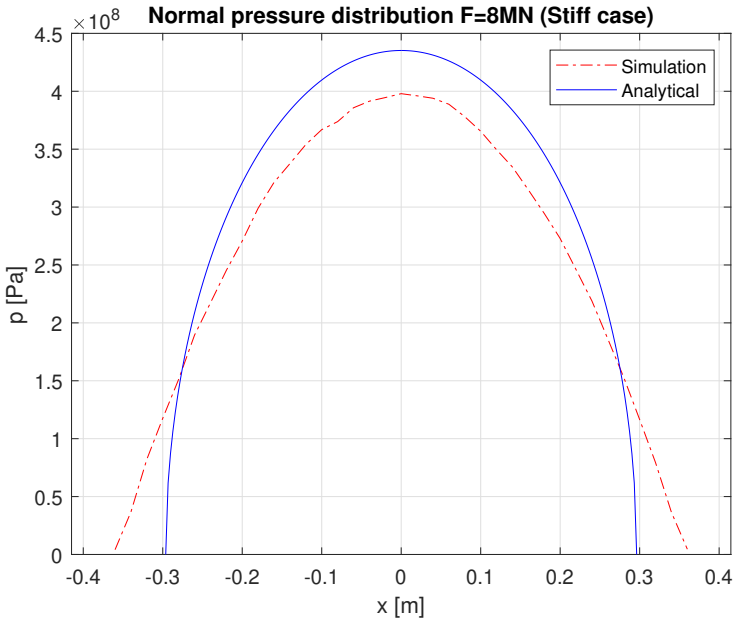

Figure 4.6: Pressure distribution - $F_n = 8$MN (stiff case)

4.2 Paraboloid indenter - elastic extension results

In order to further improve the results of the simulations, the elastic extension PCM was implemented for both material stiffness parameters $E = 3.5$MPa and $E = 210$GPa. For both cases, two different boundary conditions were examined and the results compared with the rigid scenarios. The simulation setup and boundary conditions are described in section 3.1.4.

Due to the deformation occurring on both bodies, it is no longer viable to use the same approach with the modified Young's modulus as in the rigid body simulations. Both the foundation layers now carry the non-modified value of E. The layer thickness h was set by iteration. The final values used for the simulations can be seen in table 4.6

Table 4.6: Elastic foundation layer parameters elastic PCM simulations

Boundary condition	$E_1 = E_2$	$v_1 = v_2$	$h_1 = h_2$ [m]
BC-1	3.5 MPa	0.3	0.35
BC-2	3.5 MPa	0.3	0.27
BC-1	210 GPa	0.3	0.054
BC-2	210 GPa	0.3	0.054

4.2.1 Elastic extension results - soft case

The behavior of the elastic extension PCM was first observed using the material with Young's modulus $E = 3.5\text{MPa}$. The results with the boundary condition set to only the opposite surface of the contact surface (BC-1) can be seen in figure 4.7 and the results with the boundary condition set to every surface apart from the contact surface (BC-2) can be seen in figure 4.8. These results indicate, that the use of the elastic extension can be cumbersome. In our particular case, it proved to be beneficial not to include the inertia relief modes in the simulation setup. The elastic extension did not significantly impact the results in the case of BC-1. In the case of BC-2, the impact of elastic extension is much more noticeable. It also proves the necessity of understanding and choosing the desired deformation modes manually, since the default setting, "curve Flexible", provides inaccurate results. The default setting consists of 25 eigenmodes with the lowest frequency and inertia relief modes enabled. Disabling the inertia relief modes lead to a massive improvement in the accuracy, however only after manually picking the deformation modes, the most accurate result yet was achieved in terms of the shape of the pressure distribution.

These results indicate, that it is important to understand the impact the boundary conditions will have on the system. It is also beneficial to include just the eigenmodes that correspond to the expected deformation, since this will lead to increased accuracy and reduced computational time.

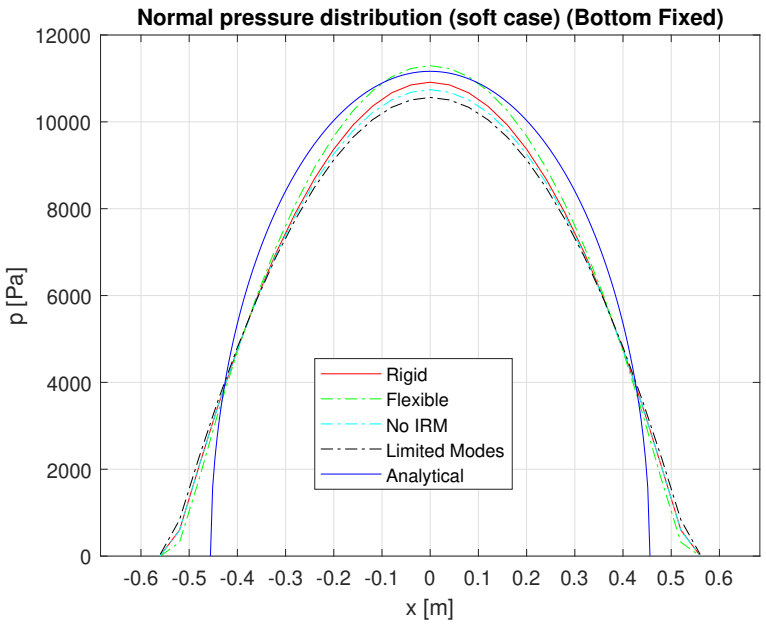

Figure 4.7: Pressure distribution BC-1 - elastic extension (soft case)

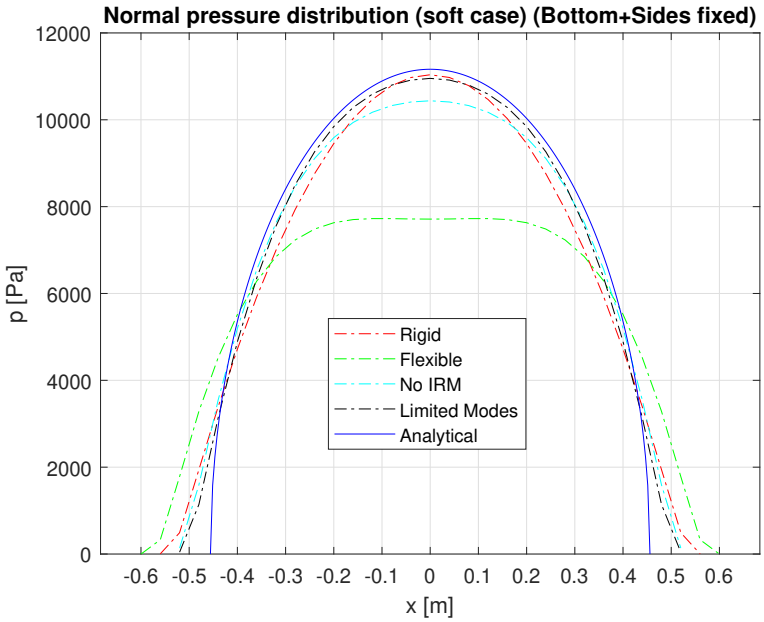

Figure 4.8: Pressure distribution BC-2 - elastic extension (soft case)

4.2.2 Elastic extension results - stiff case

In order to overcome the limitations of the rigid body PCM, the elastic extension was also implemented for the stiffer material $E = 210\text{GPa}$. However, based on the results shown in figure 4.9 and 4.10, there is little to no difference between the rigid and elastic extension simulations using the stiffer material parameters.

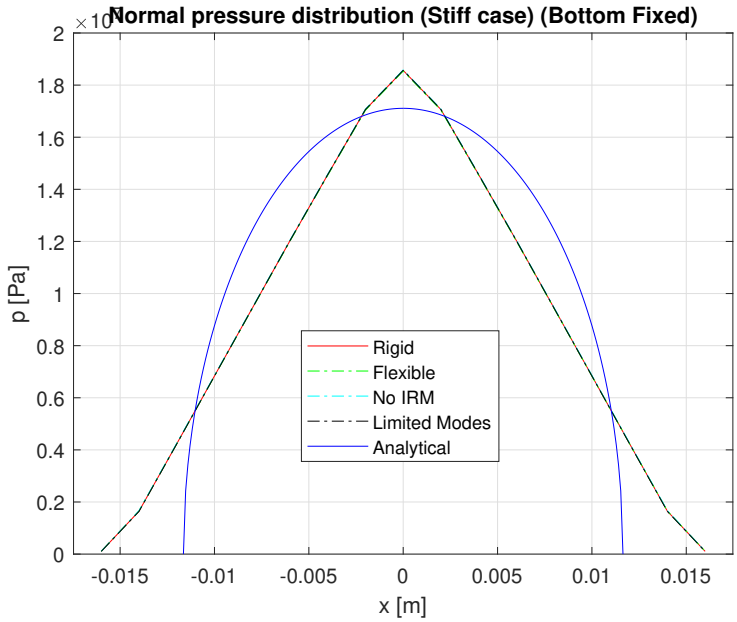

Figure 4.9: Pressure distribution BC-1 - elastic extension (stiff case)

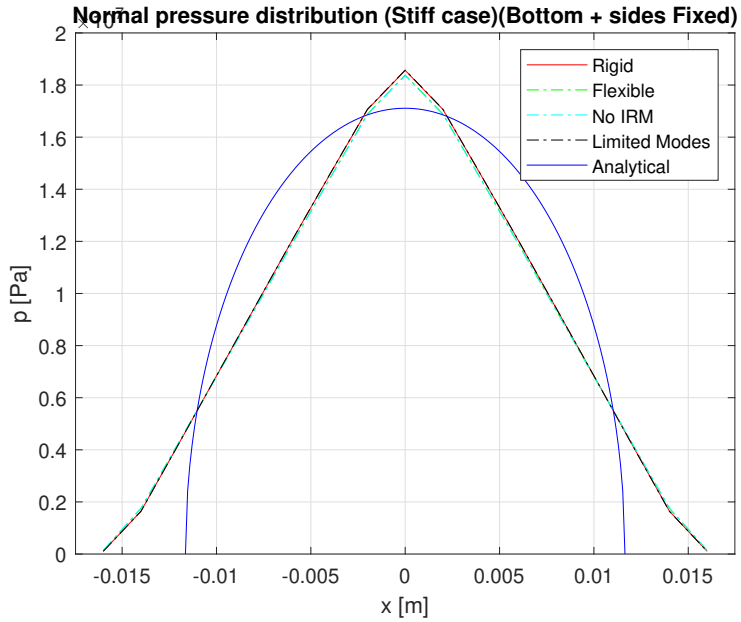

Figure 4.10: Pressure distribution BC-2 - elastic extension (stiff case)

4.3 Unworn Pole shoe on a straight rail

The results for the simulation setup described in section 3.2.1 can be seen in figures 4.11 and 4.12. Due to the use of rigid bodies and the unworn shape, the contact patch for this scenario is rather slim, only being around 0.6 mm wide. The magnitude of the normal force acting between the ploe shoe and rail was plotted in matlab and can be seen in figure 4.13. Due to the discontinuous force profile, the data was smoothened using the polyfit and polyval functions in Matlab in order to show the trend of the force distribution.

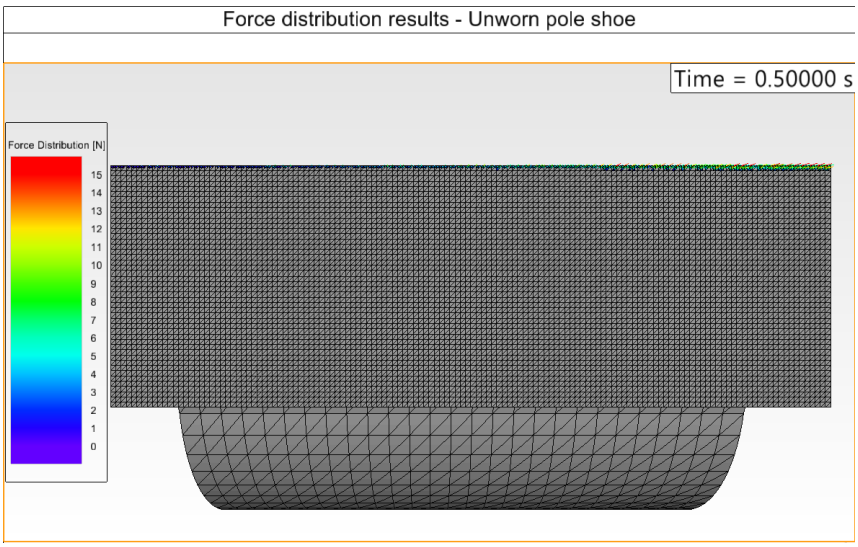

Figure 4.11: Force distribution - Unworn Pole Shoe

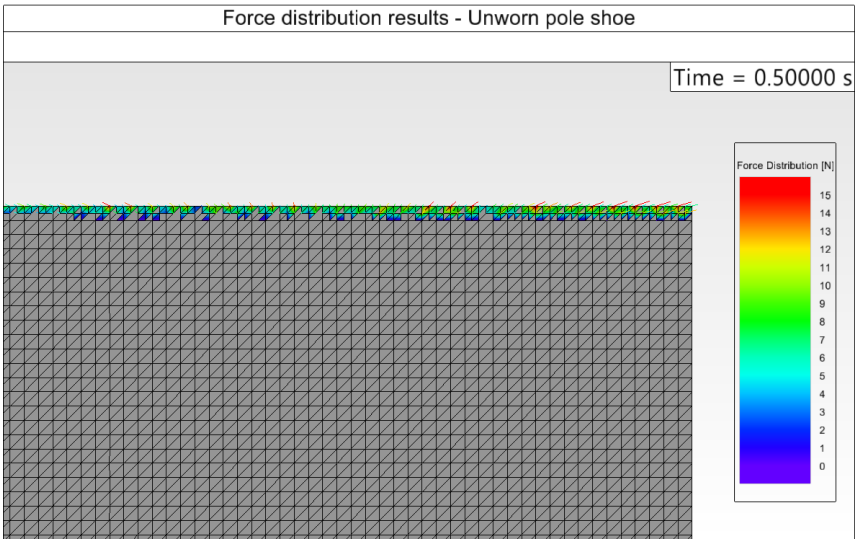

Figure 4.12: Force distribution, front of the pole shoe - Unworn Pole Shoe

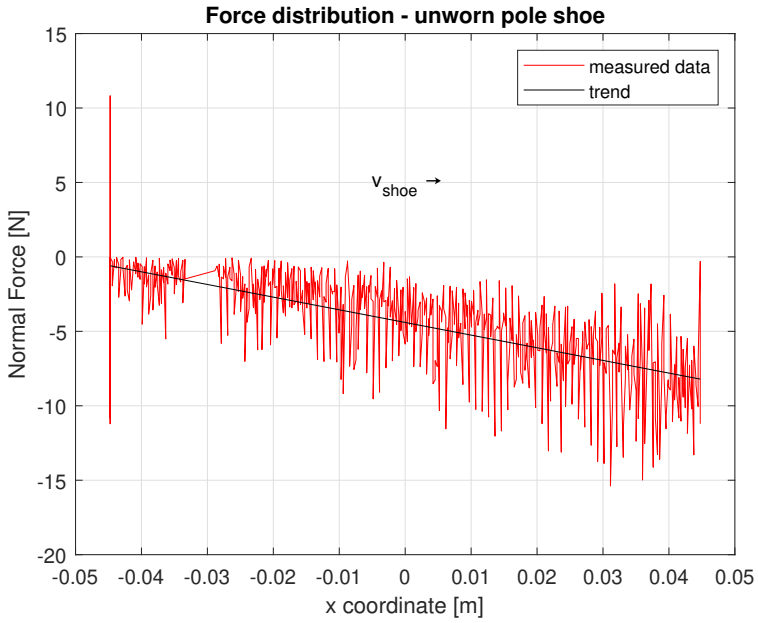

Figure 4.13: Force distribution along the pole shoe

It is tough to comment on the mesh quality, which in this case used a seed of 0.3 mm. Solver issues were experienced when trying to use a finer mesh. Using a coarser mesh results in a contact patch consisting only of one row of nodes on the pole shoe. The results however show, that the force distribution is affected by the tilting moment caused by the mounting solution for the brake shoe.

4.4 Worn pole shoe on a straight rail

This section covers the results for the worn pole shoe simulations described in section 3.2.2.

4.4.1 Mesh convergence study

In order to establish the mesh for the latter simulations, a mesh convergence study was carried out. The seed combinations used for the simulation are described in table 4.7.

Table 4.7: Seed configuration for meshes used

Seed - rail [mm]	Seed - Pole shoe [mm]
2.3	2.3
1.7	1.7
1.4	1.4
1.2	1.2
1.1	1.3
1	1.1

As can be seen from figure 4.14, the force distribution on the coarser meshes is concentrated near the middle of the contact patch. Study [11] indicates, that the peaks of the contact force should be located in the front corners of the pole shoe in the direction of travel. Using a finer mesh gives us the force distribution 4.15, which approximates the desired solution more closely. Unfortunately, we were not able to successfully finish a simulation using a finer mesh, which could have potentially lead to an even more accurate result. For this reason, the finest mesh from table 4.7 will be used for the other studies.

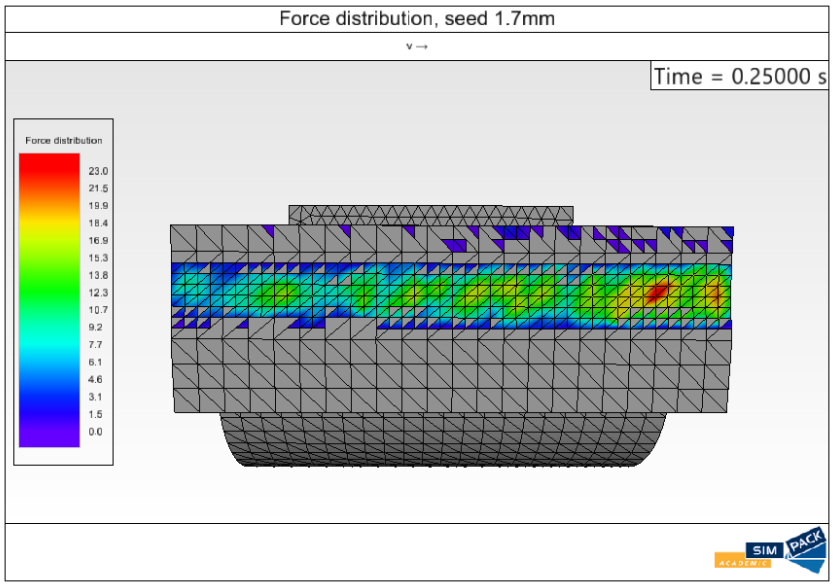

Figure 4.14: Force distribution on the pole shoe, seed 1.7mm

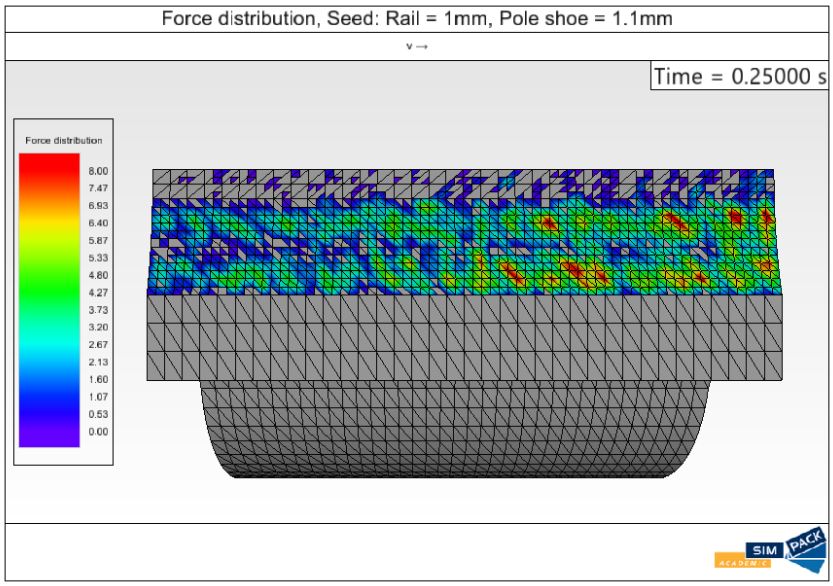

Figure 4.15: Force distribution on the pole shoe, seed: Rail = 1mm, Pole shoe = 1.1mm

It has to be noted, that the force distribution is not constant across the timesteps. Although a quasi-steady behavior was expected, the force distribution varies quite a lot. This can be seen in figures 4.16 and 4.17. Both of these timesteps occur when the overall contact force is relatively constant, however there is a significant difference in the pressure distribution. This is possibly caused by the foundation layer, more specifically the relative position of nodes on the two bodies.

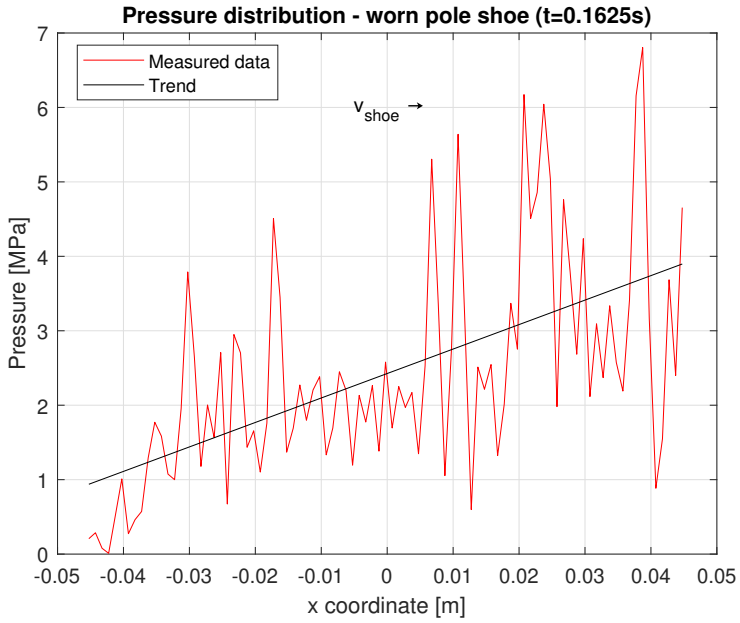

Figure 4.16: Pressure distribution, t=0.1625 s

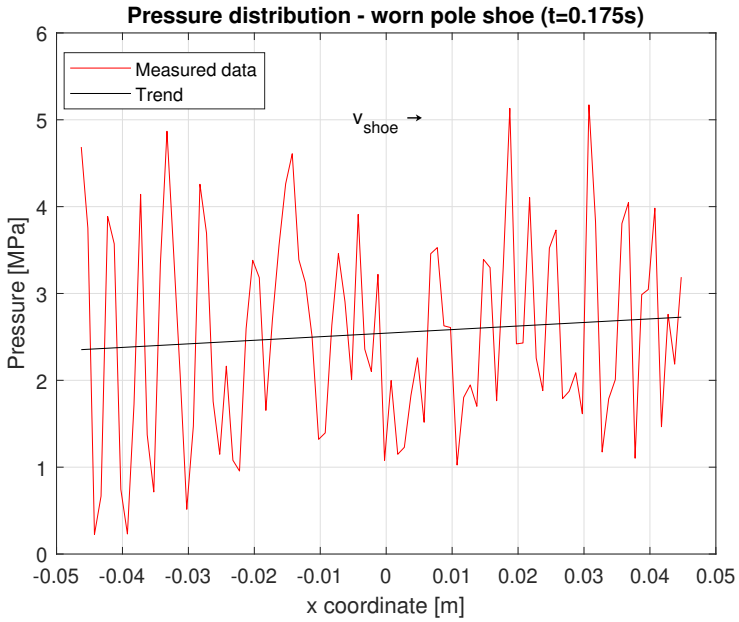

Figure 4.17: Pressure distribution, t=0.175 s

4.4.2 Solver comparison

A comparison of the different solvers available within Simpack was done with the aim of further improving the force distribution. To eliminate the transient behavior of the force distribution described in section 4.4.1, a velocity of 0.4 mm was used. Each simulation was carried out using a 1000 Hz sampling frequency with a simulation time of 1 second. A summary of the solvers used and the run time for each solver is presented in table 4.8.

Table 4.8: Comparison of solvers, worn pole shoe

Solver	Simulation status	Run Time
SODASRT 2	Finished	7 h 11 min
RADAU 5	Finished	67 h 40 min
SOBDF 2	Finished	12 h 57 min
Fixed timestep	Failed	-
LSODE	Failed	-
DOPRI 5	Failed	-

Apart from the significant increase in the run time of the simulation, there is no difference between the results. The force distributions for the finished simulations can be found in appendix C. For this reason, we will continue using the default SODASRT 2 solver for simulations in 4.4.3.

4.4.3 Impact of μ

As a last study done using the worn pole shoe, results of simulations using different friction coefficients μ were compared. Values 0, 0.2, 0.4, 0.5 and 0.6 were used in

the simulations. The results below confirm the expected behavior, that a higher coefficient of friction leads to more force being applied in the front of the pole shoe. Results in figure 4.21 using the friction coefficient $\mu = 0.5$ can be directly compared to those from study [11]. Although we are limited to the use of a rigid body, the contact patch is approximated fairly well. In a similar manner as in [11], the forces are limited to the front half of the model. The FEA solution does not have any contact in the rear half of the pole shoe due to deformation. This is not achievable using the rigid body PCM, however the contact force occurring in the rear part of the pole shoe is very low.

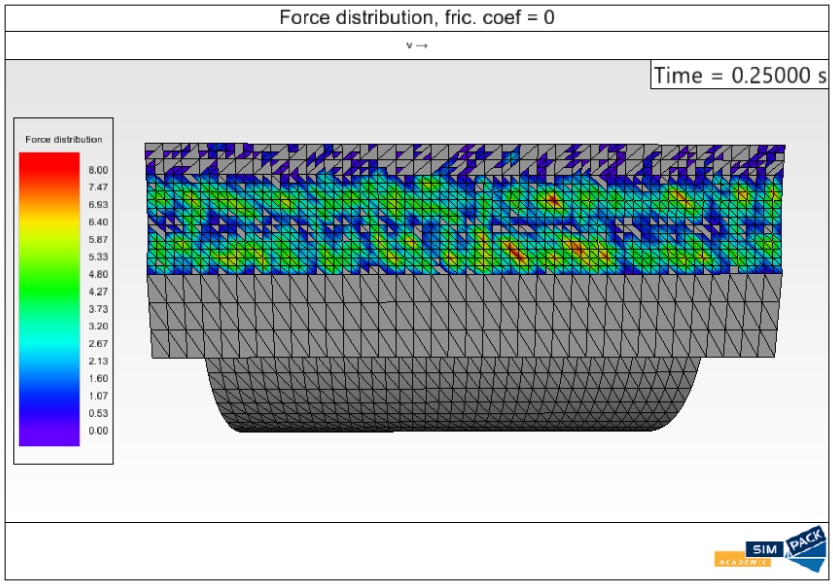

Figure 4.18: Force distribution, $\mu = 0$

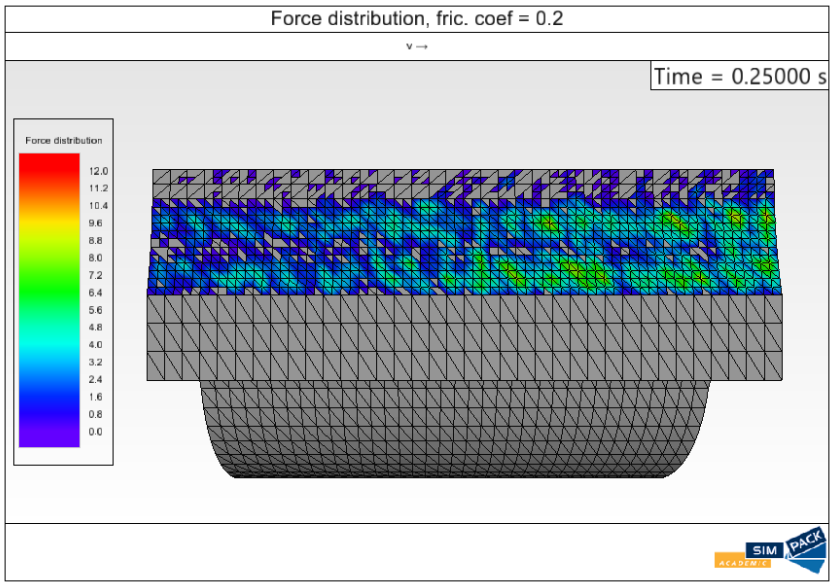

Figure 4.19: Force distribution, $\mu = 0.2$

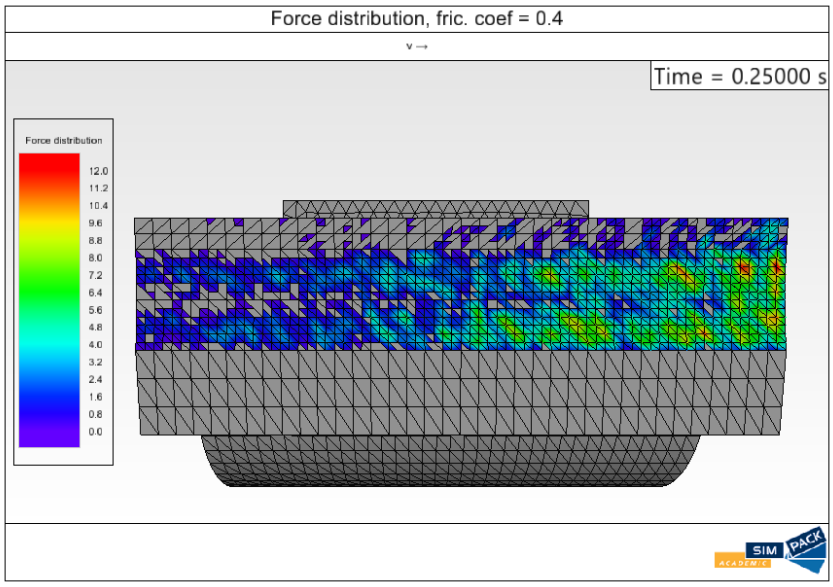

Figure 4.20: Force distribution, $\mu = 0.4$

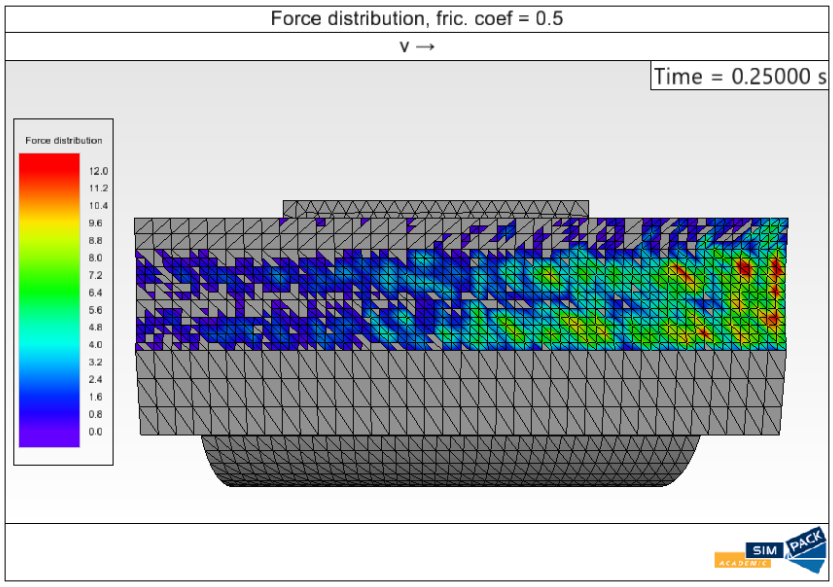

Figure 4.21: Force distribution, $\mu = 0.5$

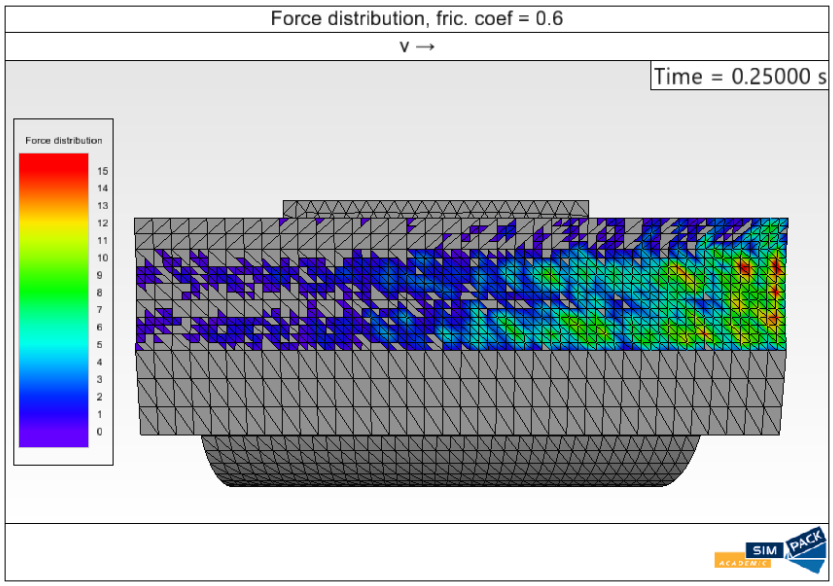

Figure 4.22: Force distribution, $\mu = 0.6$

5
Conclusion

Two scenarios were examined and evaluated in order to assess the usability of the Polygonal Contact Model for magnetic track brake simulations. The results of the paraboloid indenter showed some flaws with the use of the PCM. Although the results for the softer material achieved sufficient accuracy in terms of pressure distribution and contact patch size, the use of the stiffer material introduced some issues. The issues regarding the accuracy and computational stability mentioned in [7] were proven correct. The results of simulations using the stiffer material parameters did not resemble the analytical solution with the desired accuracy. The impact of the elastic extension of PCM has shown negligible impact using the stiffer material. The utilization of the elastic extension PCM can improve the results, given the deformation is significant, but the extra preprocessing steps, increased computational effort and complex configuration options compromise its usability.

The choice of the foundation layer thickness also turned out to be problematic, since the proposed value based on equation 3.7 produced faulty results when using the stiffer material parameters. This shows the necessity of setting the foundation layer thickness by comparison of results to other simulations or an analytical solution.

Further, the results of the pole shoe simulations indicate that it is difficult to study the force distribution when there is velocity introduced into the system. The force distribution does not reach a quasi-steady state and varies heavily between timesteps.

During the simulations of the worn pole shoe, convergence issues and simulation crashes were observed. This was most likely caused by the conforming surfaces of the pole shoe and the rail head, since it is also ackowledged in [7].

Based on these observation, it was concluded that the version of PCM implemented within Simpack does not produce results accurate enough for local force distribution studies. Possible studies, that could be carried out in the future could examine the behavior of the updated PCM mentioned in [7], however this version has not yet been implemented in Simpack. Future studies could also verify the negligible impact of the elastic extension PCM on the pole shoe simulations and observe the behavior of PCM in dynamic simulations, for example the interaction between a pole shoe and a rail going over switches and crossings.

Bibliography

[1] Evert Andersson et al. *Rail Systems and Rail Vehicles, Part 2: Rail Vehicles*. 2018. ISBN: 978-91-7729-736-9.

[2] Dassault Systèmes. *Abaqus 2024 Documentation*. Version 2024. 2024.

[3] Dassault Systèmes. *Simpack 2025 Documentation*. Version 2025. 2025.

[4] Saeed Ebrahimi, G Hippmann, and P Eberhard. "Extension of the polygonal contact model for flexible multibody systems". In: *International Journal of Applied Mathematics and Mechanics* 1 (Jan. 2005).

[5] Dipl.-Ing. Gerhard Hippmann. "MODELLIERUNG VON KONTAKTEN KOMPLEX GEFORMTER KÖRPER IN DER MEHRKÖRPERDYNAMIK". PhD thesis. TU Wien, 2004.

[6] Gerhard Hippmann. "An Algorithm for Compliant Contact Between Complexly Shaped Bodies". In: *Multibody System Dynamics* 12.4 (2004), pp. 345–362. DOI: 10.1007/s11044-004-2513-4. URL: https://doi.org/10.1007/s11044-004-2513-4.

[7] Gerhard Hippmann. "Polygonal contact model revisited: notes on usage and improved implementation". In: *Multibody System Dynamics* 60.2 (2024), pp. 219–231. ISSN: 1573-272X. DOI: 10.1007/s11044-023-09895-8. URL: https://doi.org/10.1007/s11044-023-09895-8.

[8] K. L. Johnson. *Contact Mechanics*. Cambridge University Press, 1985, pp. 104–106.

[9] Emin Kocbay. *Personal communication*. Verbal comunication, May 22, 2025. 2025.

[10] Emin Kocbay et al. "Efficient and simplified numerical contact model for the braking simulation of a magnetic track brake". In: *Meccanica* 60.2 (2025), pp. 195–216. ISSN: 1572-9648. DOI: 10.1007/s11012-024-01926-8. URL: https://doi.org/10.1007/s11012-024-01926-8.

[11] Andreas Pavicsics. "Finite element modelling of the frictional sliding contact within the application of the magnetic track brake". MA thesis. TU Wien, 2024.

[12] Valentin Popov, Markus Heß, and Emanuel Willert. *Handbook of Contact Mechanics: Exact Solutions of Axisymmetric Contact Problems*. Apr. 2019. ISBN: 978-3-662-58708-9. DOI: 10.1007/978-3-662-58709-6.

[13] Milla Vehviläinen et al. "Adapting geometry-based polygonal contacts for simulating faulty rolling bearing dynamics". In: *Mechanism and Machine Theory* 192 (2024), p. 105552. ISSN: 0094-114X. DOI: https://doi.org/10.1016/j.mechmachtheory.2023.105552. URL: https://www.sciencedirect.com/science/article/pii/S0094114X23003233.

[14] G. Zachmann. “Rapid collision detection by dynamically aligned DOP-trees”. In: *Proceedings. IEEE 1998 Virtual Reality Annual International Symposium (Cat. No.98CB36180)*. 1998. DOI: 10.1109/VRAIS.1998.658428.

A

Appendix A

This appendix contains settings connected to the setup of the simulations.

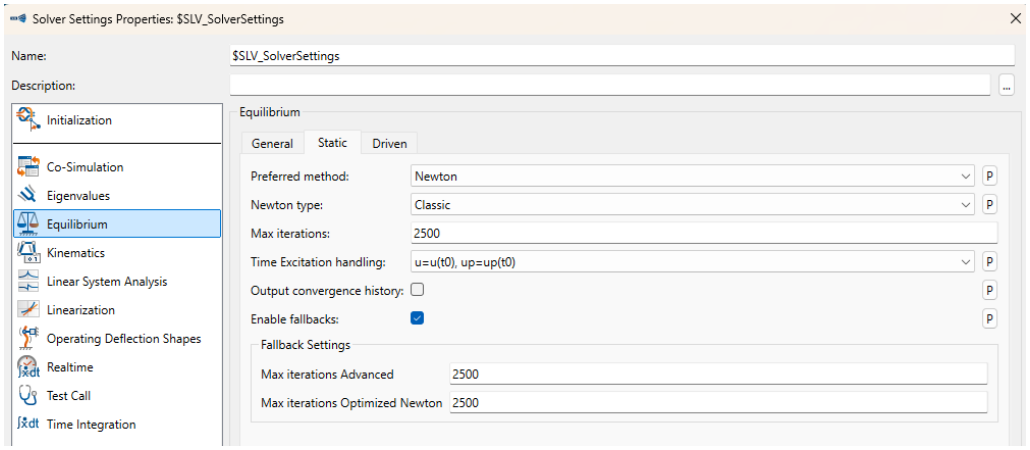

Figure A.1: Settings of the Equilibrium solver

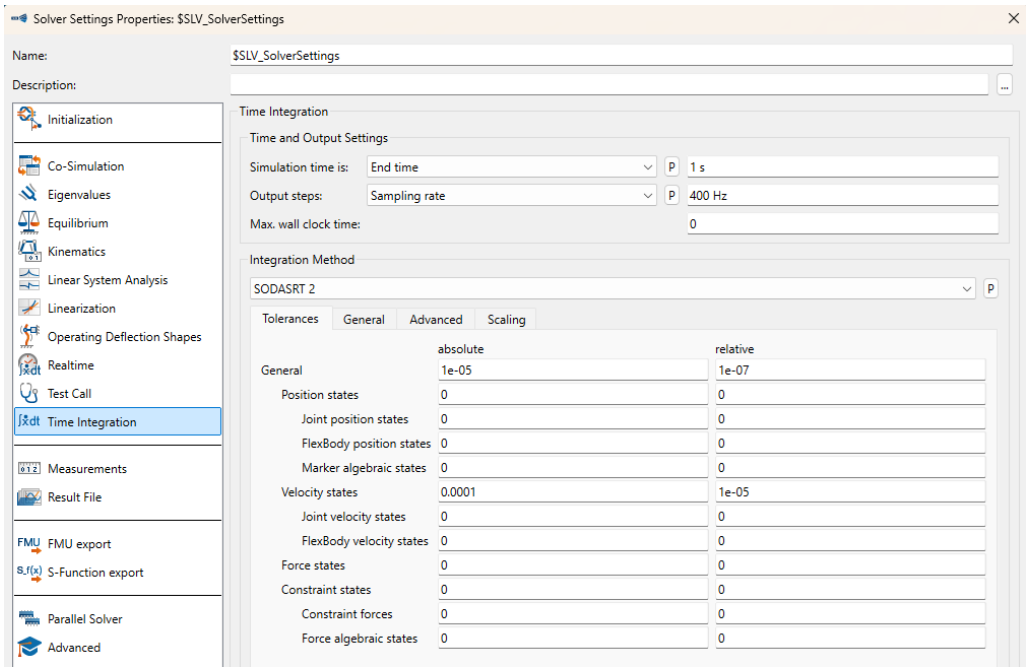

Figure A.2: Settings of the Time integration solver

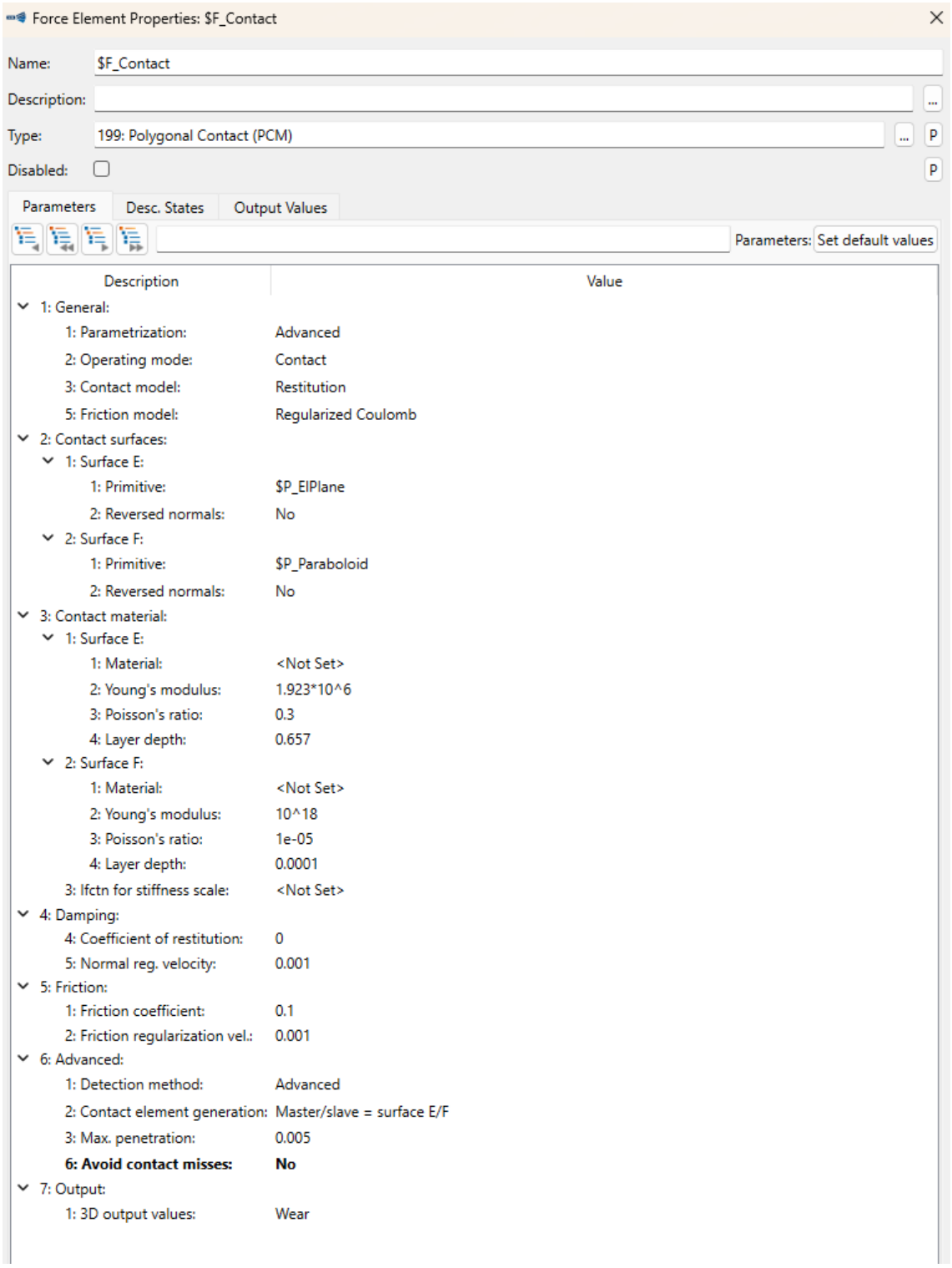

Figure A.3: Settings of the PCM force element in Simpack

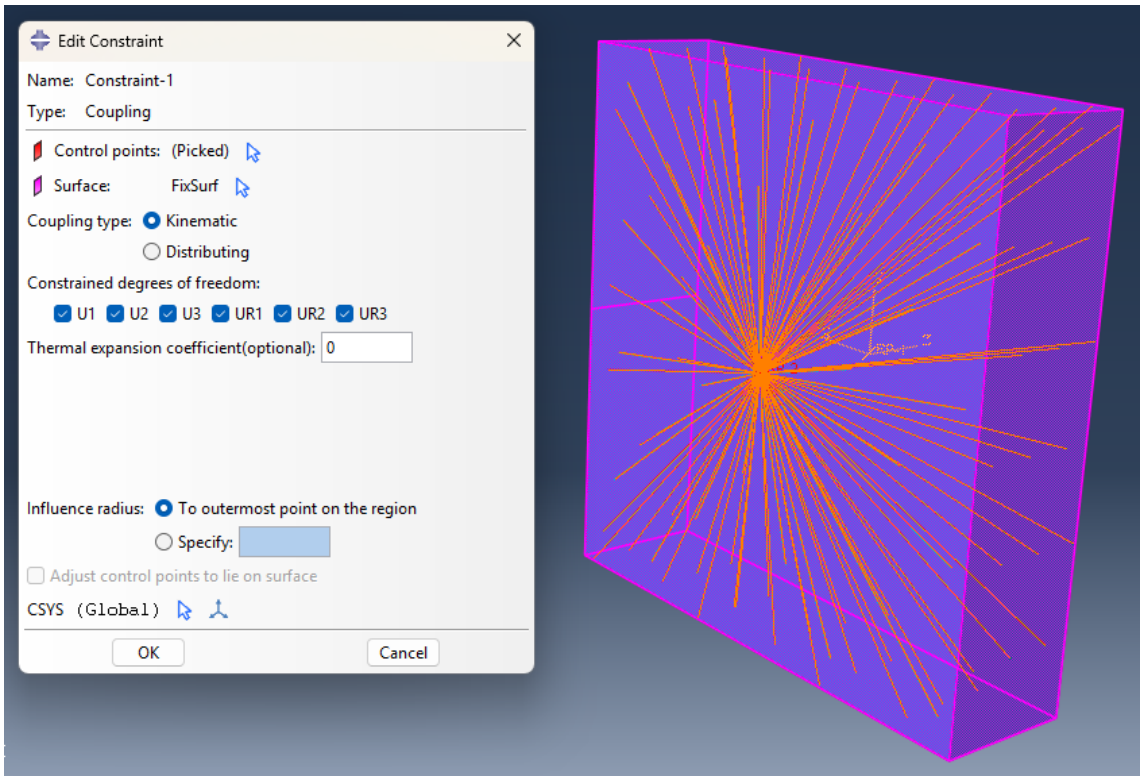

Figure A.4: Coupling settings-Halfspace, all surfaces fixed apart from contact surface (BC-2)

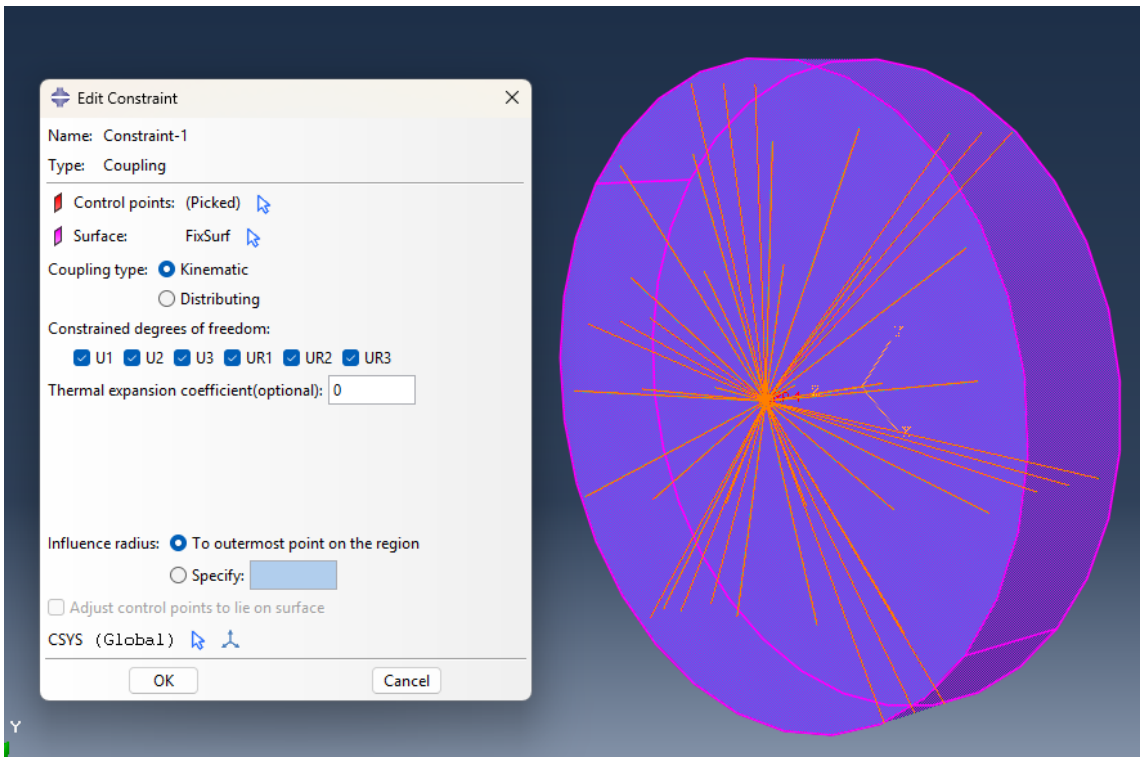

Figure A.5: Coupling settings - Paraboloid, all surfaces fixed apart from contact surface (BC-2)

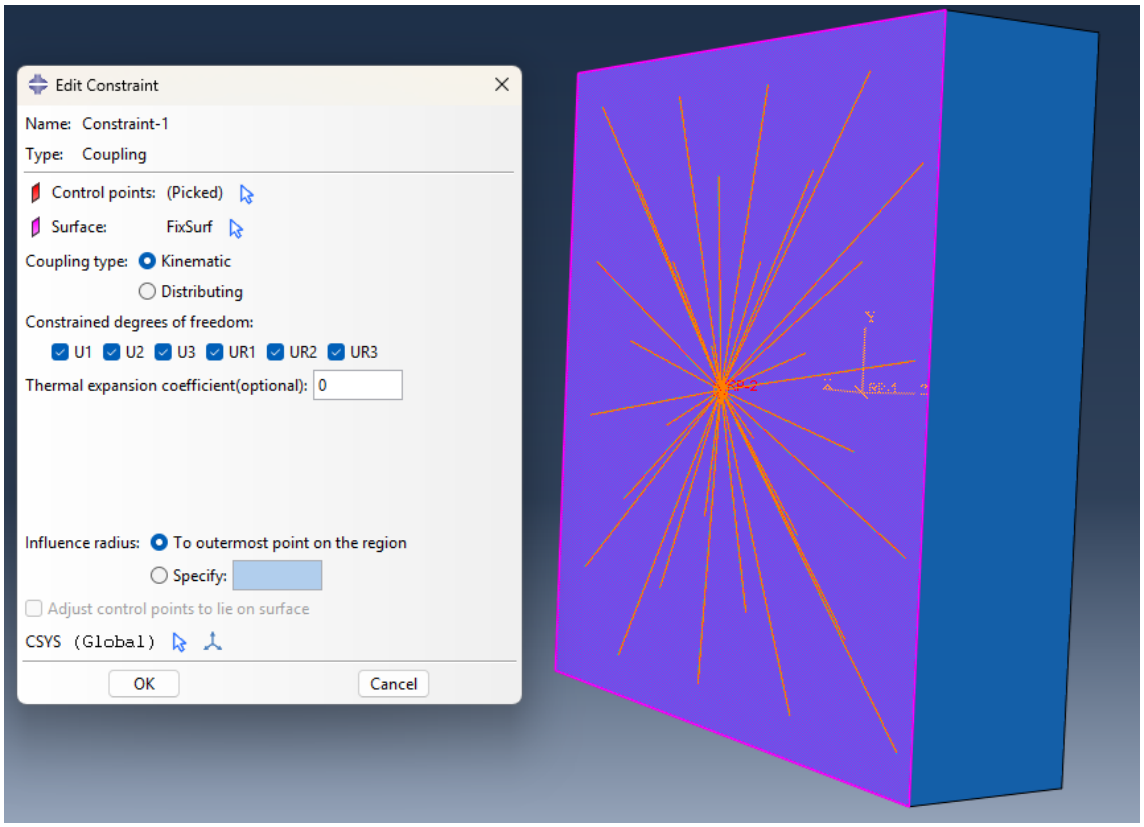

Figure A.6: Coupling settings - Halfspace, opposite surface fixed (BC-1)

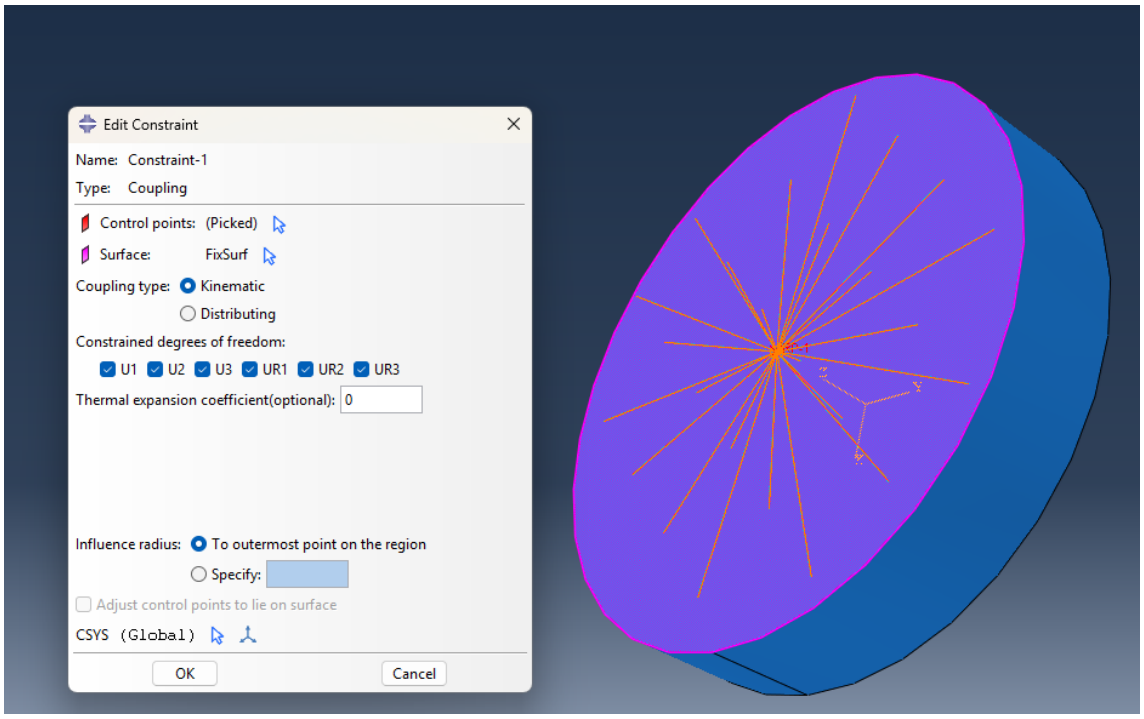

Figure A.7: Coupling settings - Paraboloid, opposite surface fixed (BC-1)

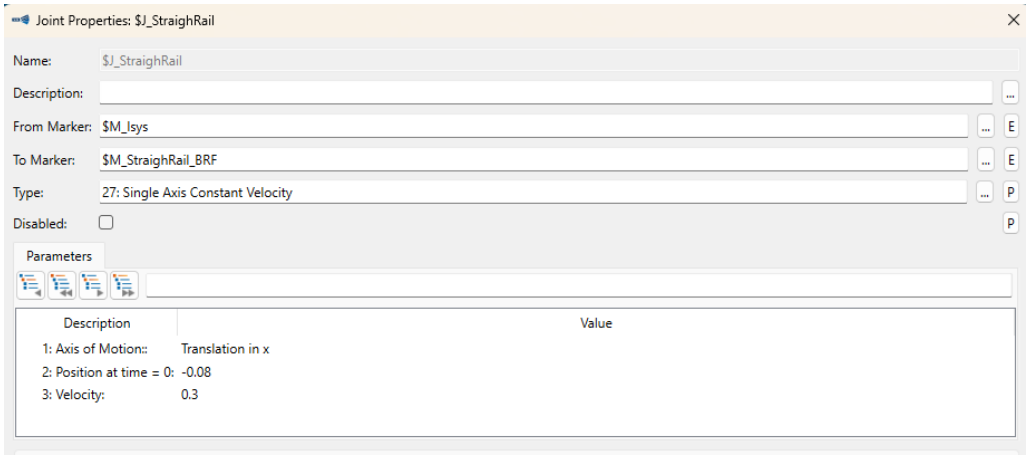

Figure A.8: Rail joint settings (Unworn Pole Shoe simulation)

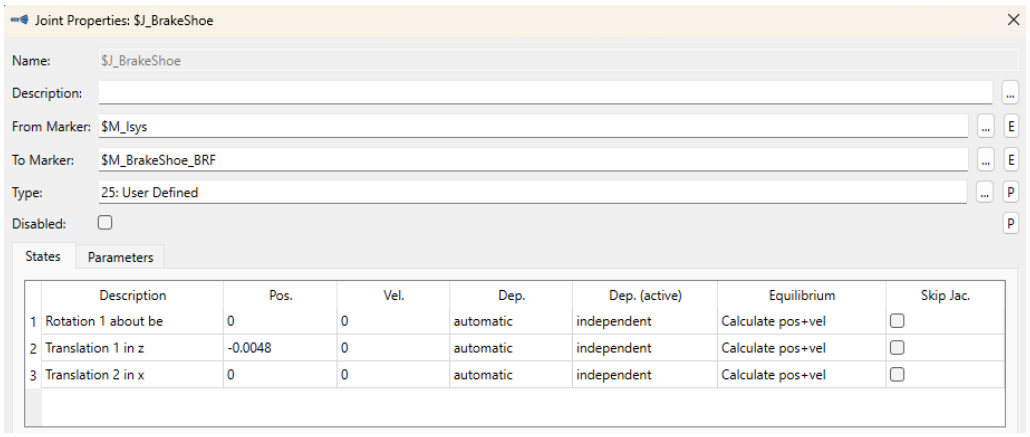

Figure A.9: Pole Shoe joint settings (Unworn Pole Shoe simulation)

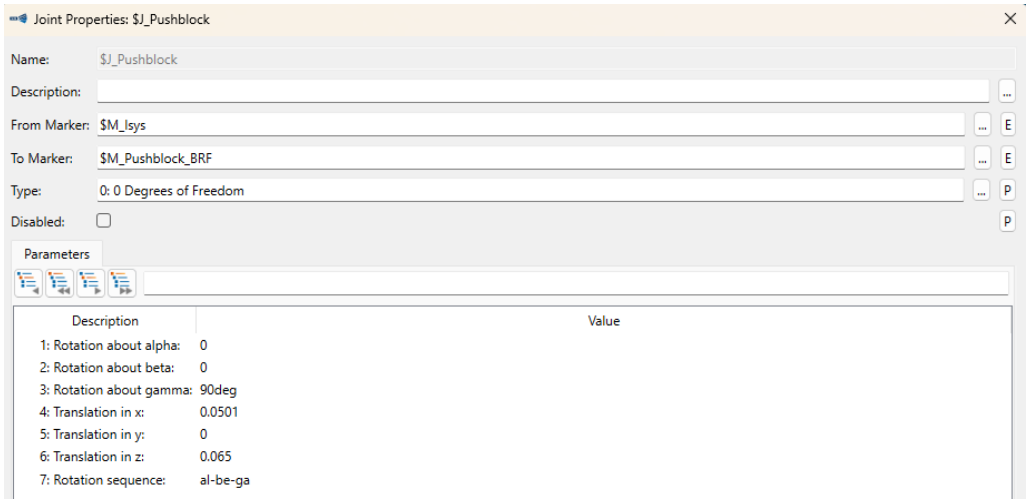

Figure A.10: Push Block joint settings (Unworn Pole Shoe simulation)

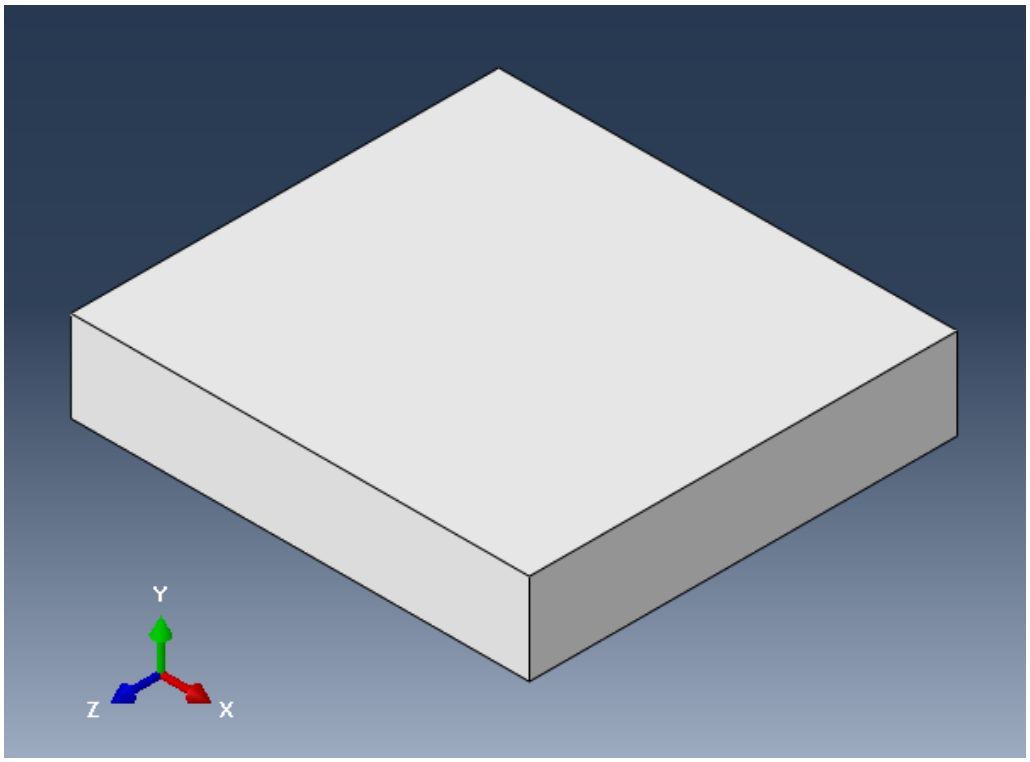

Figure A.11: Push Block Geometry

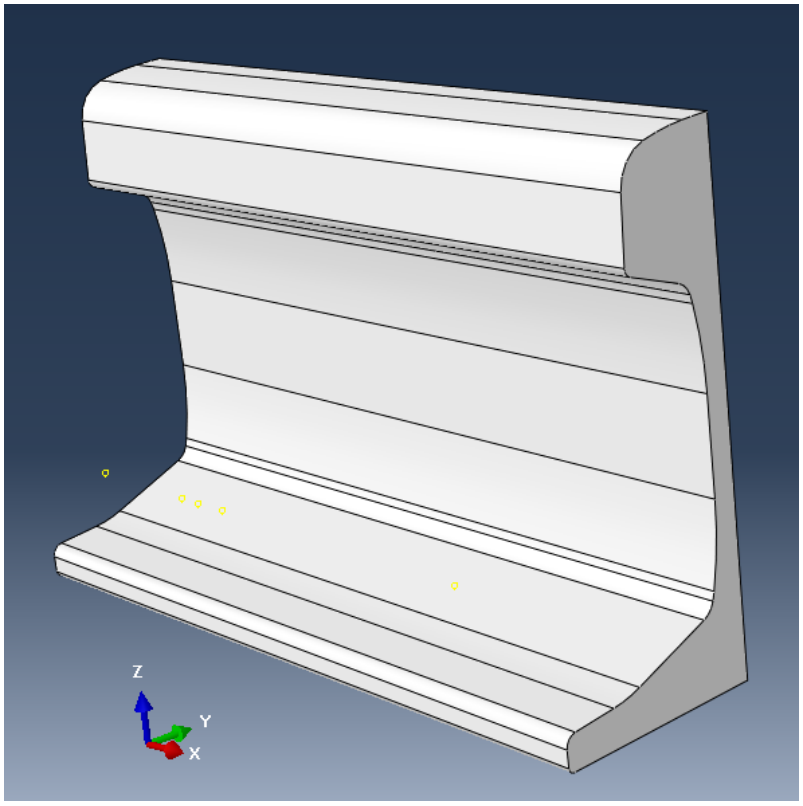

Figure A.12: Rail Geometry, view from angle

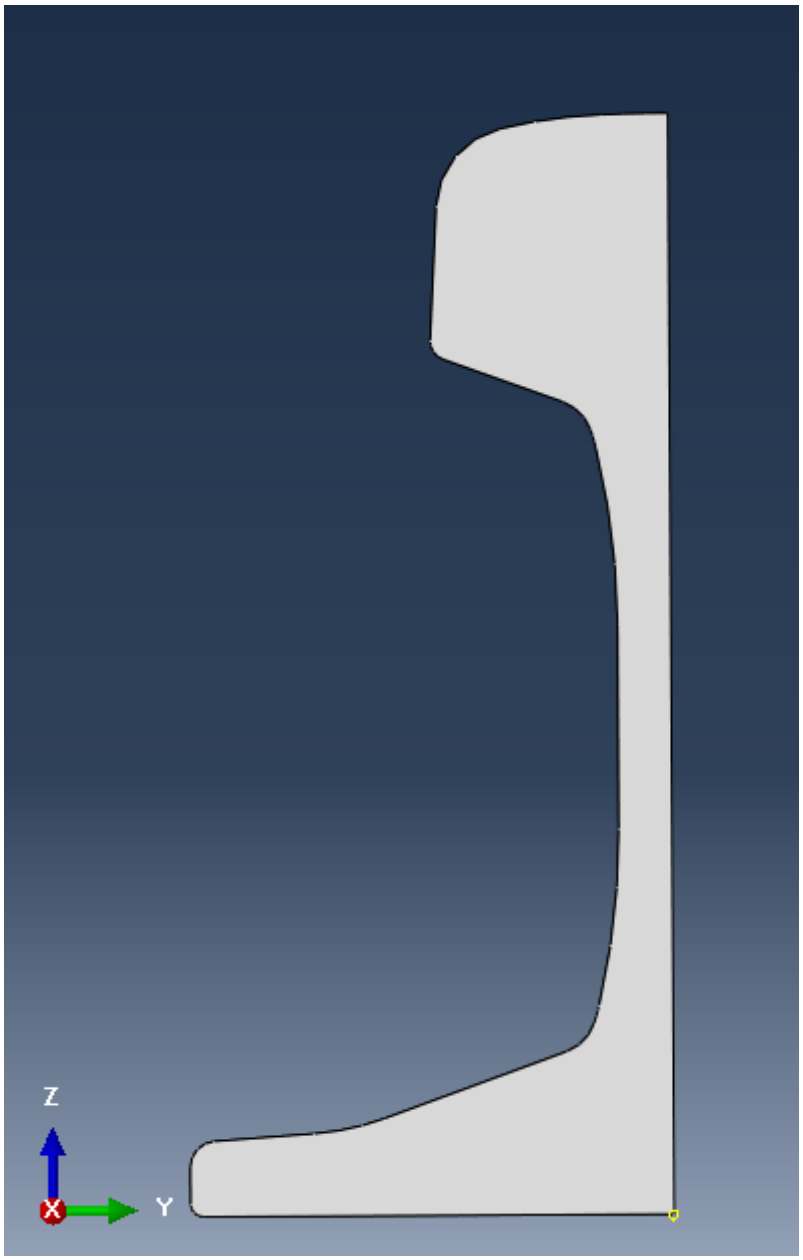

Figure A.13: Rail Geometry, view from the front

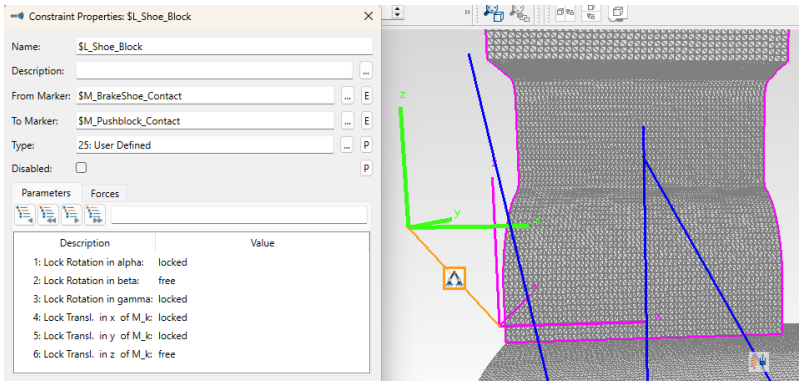

Figure A.14: Kinematic constraint settings (worn pole shoe simulations)

B

Appendix B

This appendix contains additional results of the paraboloid indenter scenario. Pressure distribution plots of the simulations studying the influence of applied force for both soft and stiff cases are part of this appendix. Results of the mesh convergence for the stiff case is also a part of this appendix. Pressure distribution plots of the simulations studying the influence of applied force for both soft and stiff cases are part of this appendix. Results of the mesh convergence for the stiff case is also a part of this appendix.

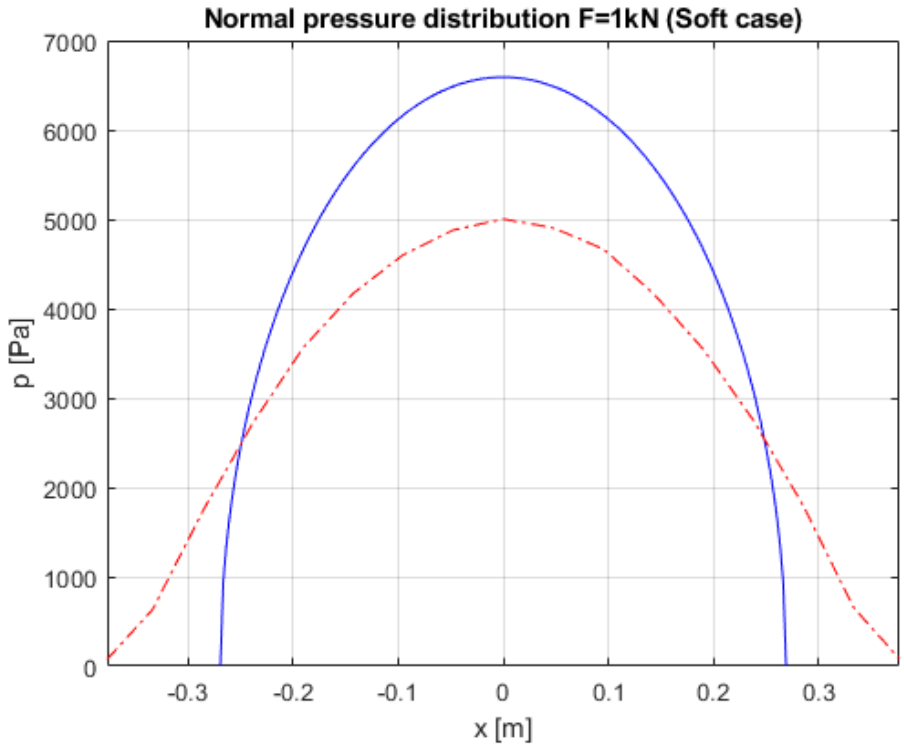

Figure B.1: Pressure distribution - $Fn = 1$kN (soft case)

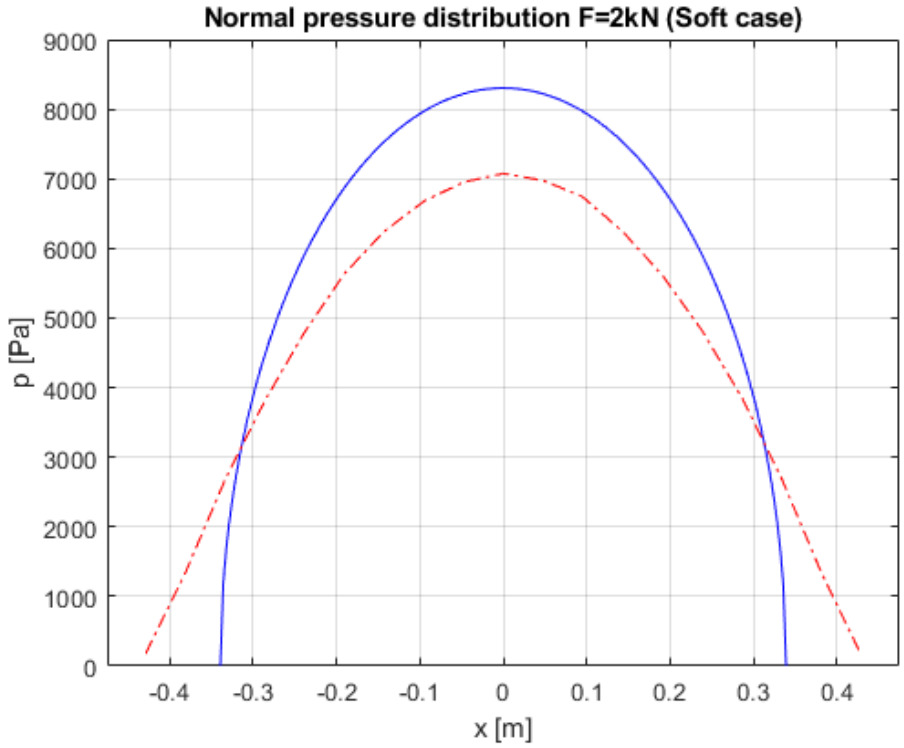

Figure B.2: Pressure distribution - $Fn = 2$kN (soft case)

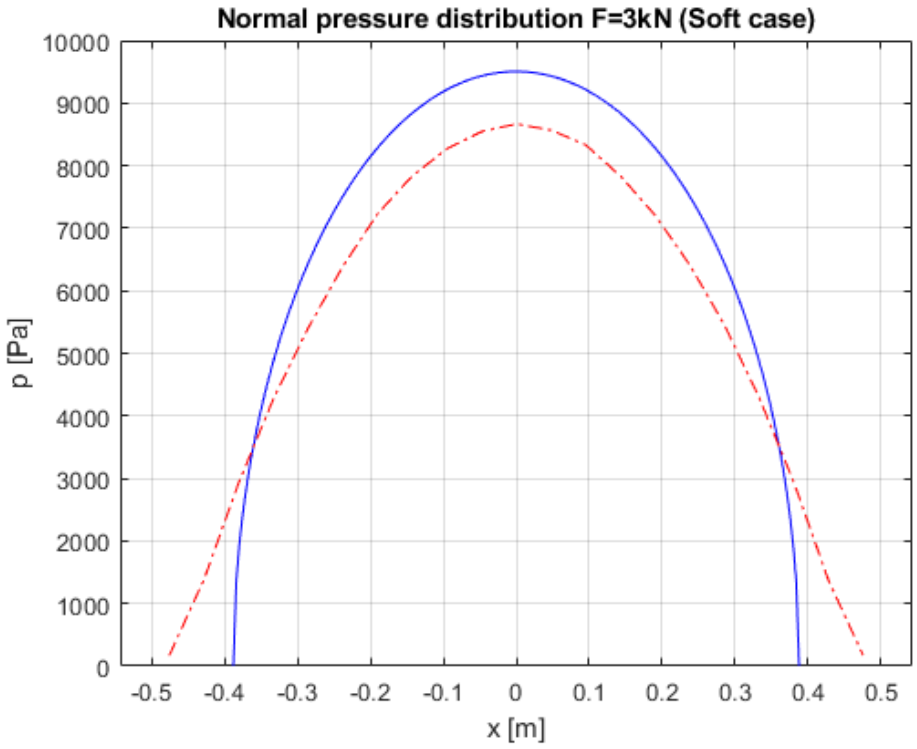

Figure B.3: Pressure distribution - $Fn = 3$kN (soft case)

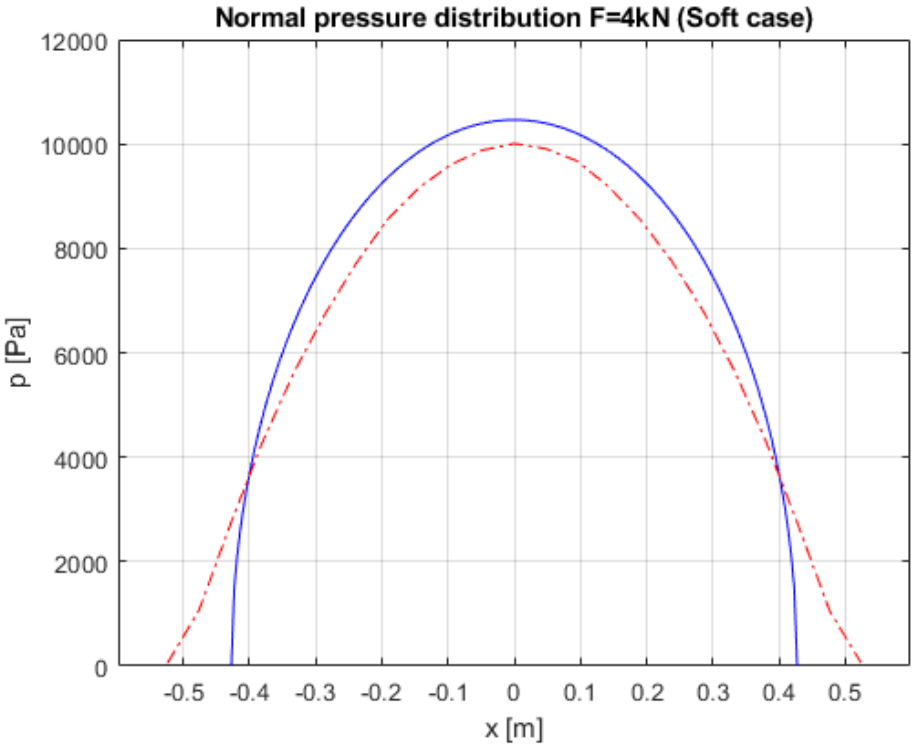

Figure B.4: Pressure distribution - $Fn = 4$kN (soft case)

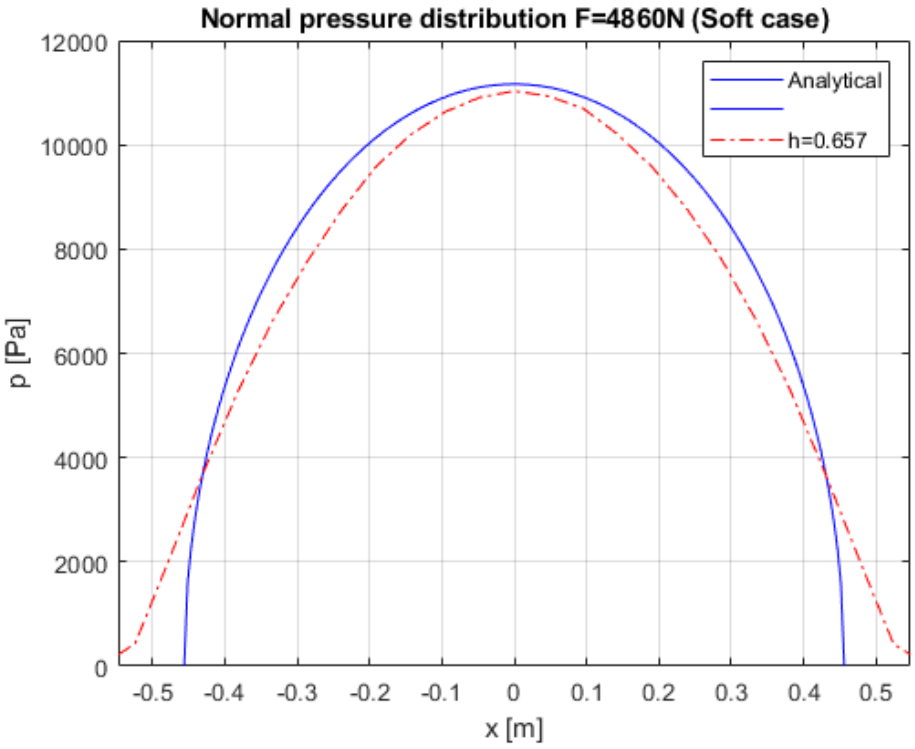

Figure B.5: Pressure distribution - $Fn = 4.86$kN (soft case)

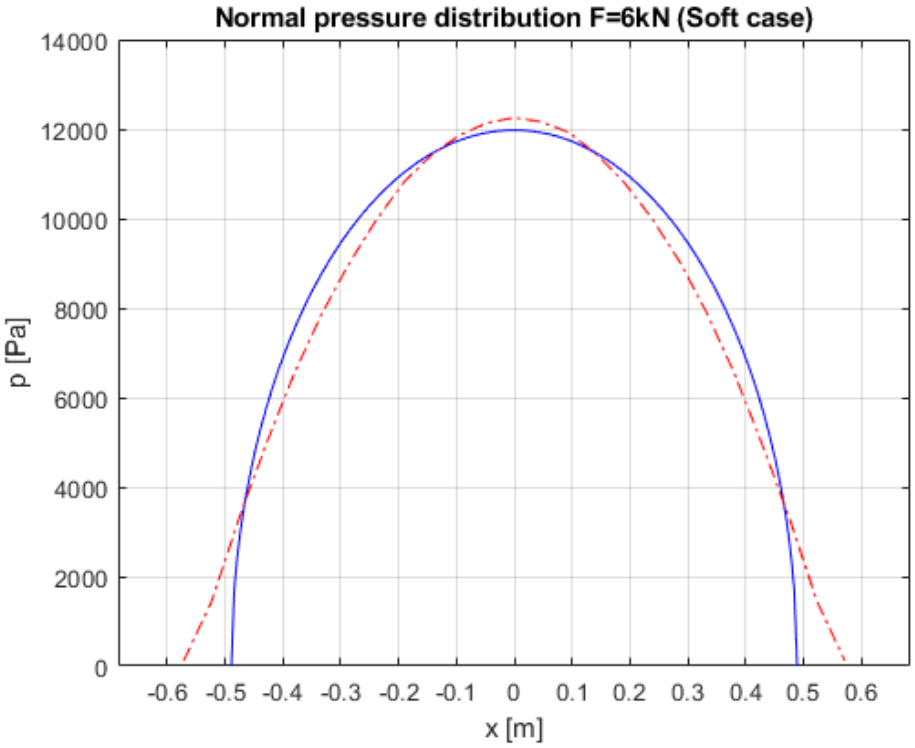

Figure B.6: Pressure distribution - $Fn = 6$kN (soft case)

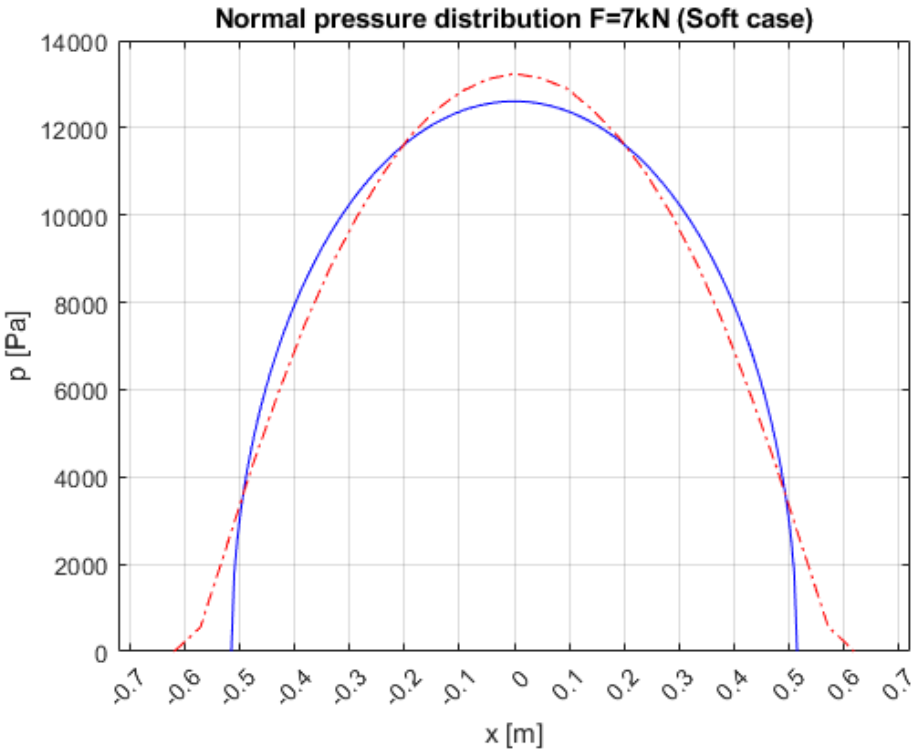

Figure B.7: Pressure distribution - $Fn = 7$kN (soft case)

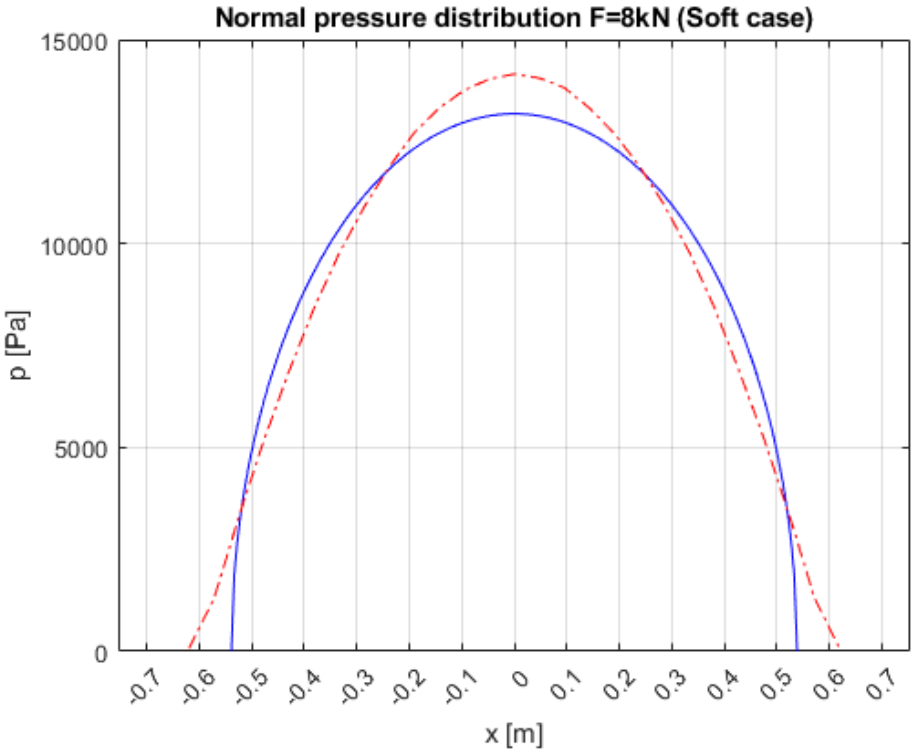

Figure B.8: Pressure distribution - $Fn = 8$kN (soft case)

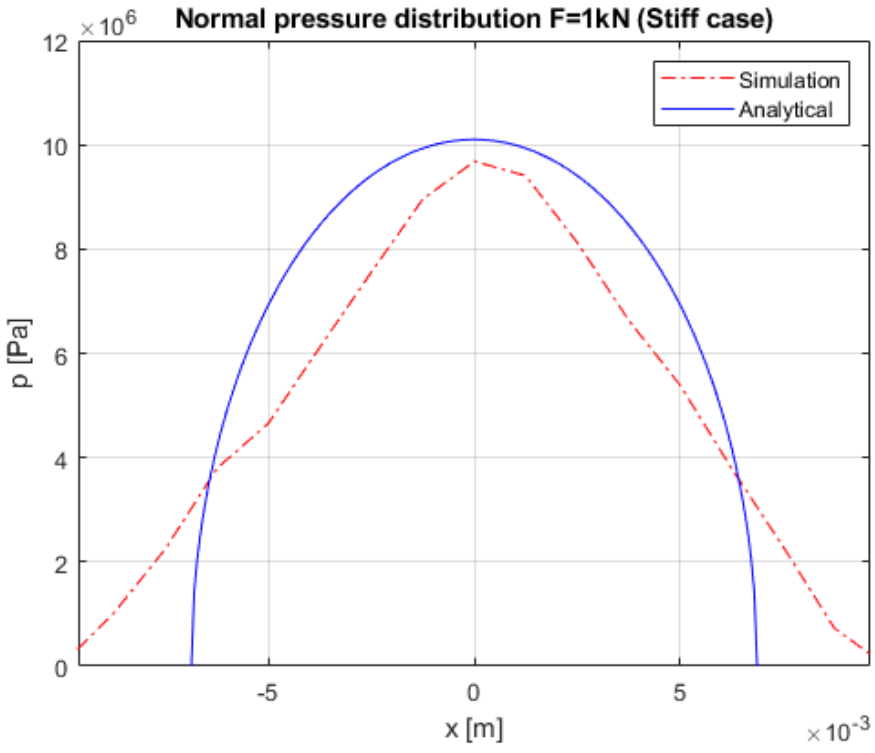

Figure B.9: Pressure distribution - $Fn = 1$kN (stiff case)

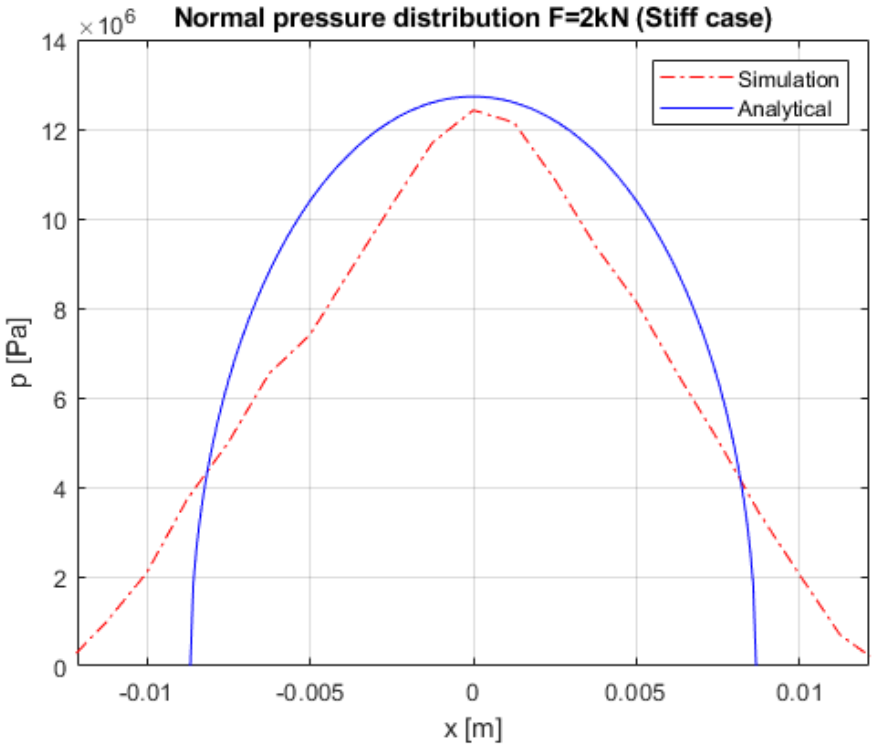

Figure B.10: Pressure distribution - $Fn = 2$kN (stiff case)

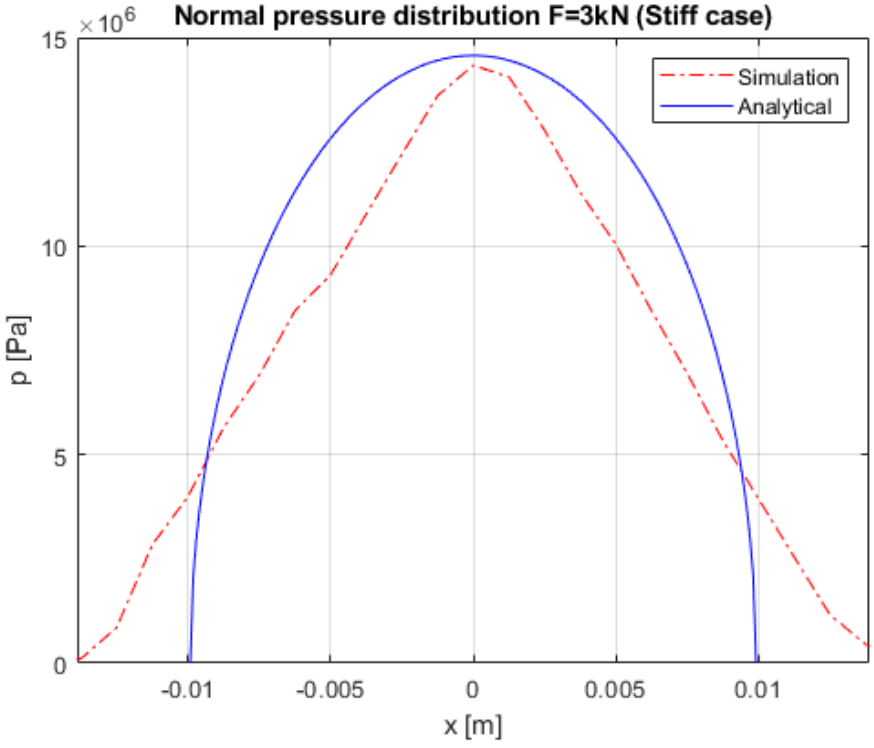

Figure B.11: Pressure distribution - $Fn = 3$kN (stiff case)

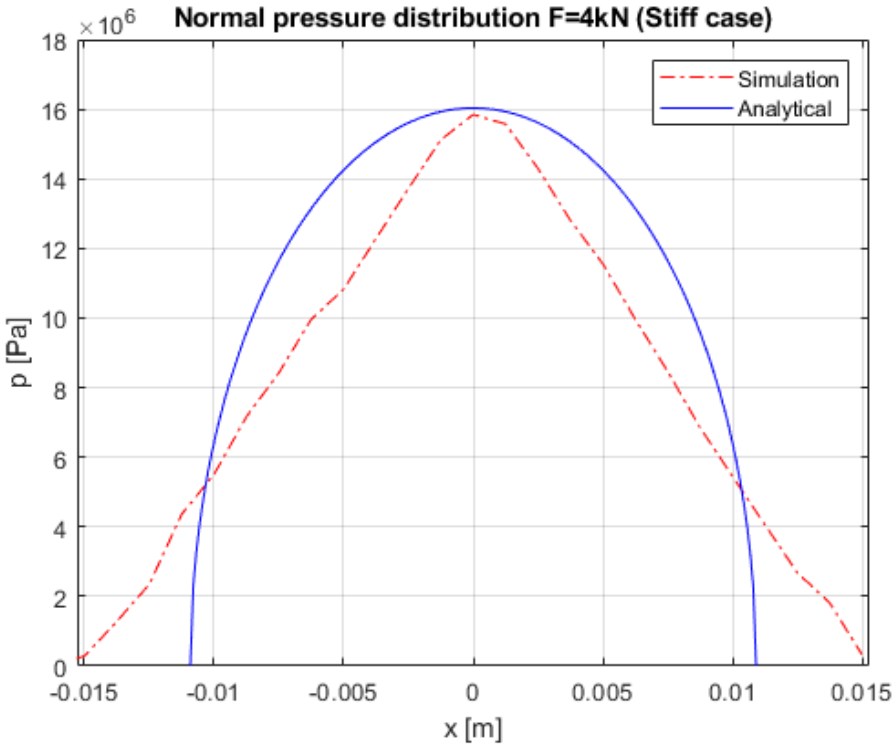

Figure B.12: Pressure distribution - $Fn = 4$kN (stiff case)

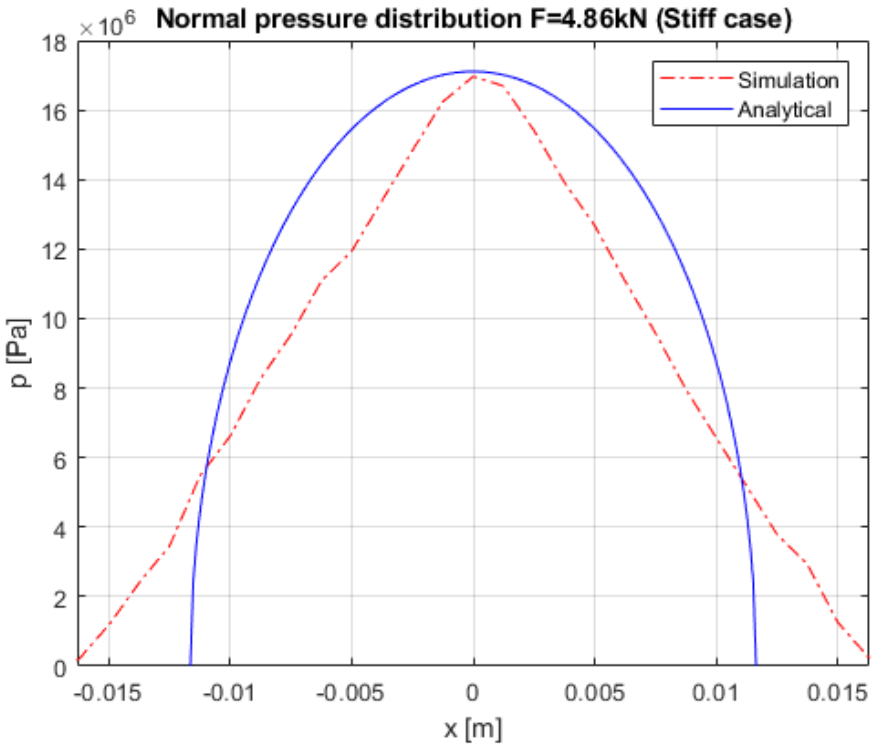

Figure B.13: Pressure distribution - $Fn = 4.86$kN (stiff case)

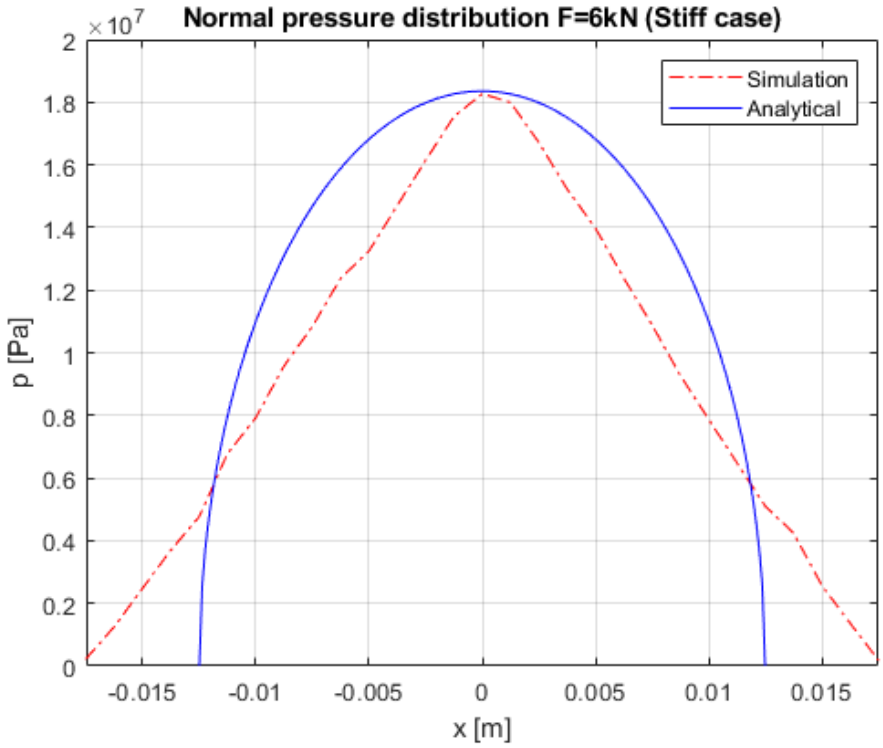

Figure B.14: Pressure distribution - $Fn = 6$kN (stiff case)

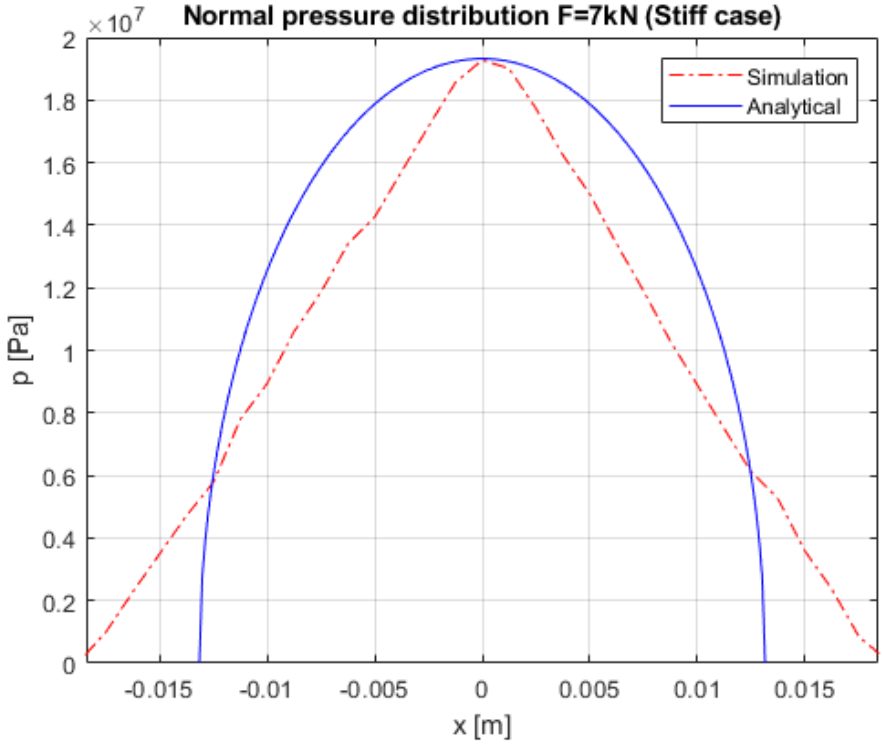

Figure B.15: Pressure distribution - $Fn = 7$kN (stiff case)

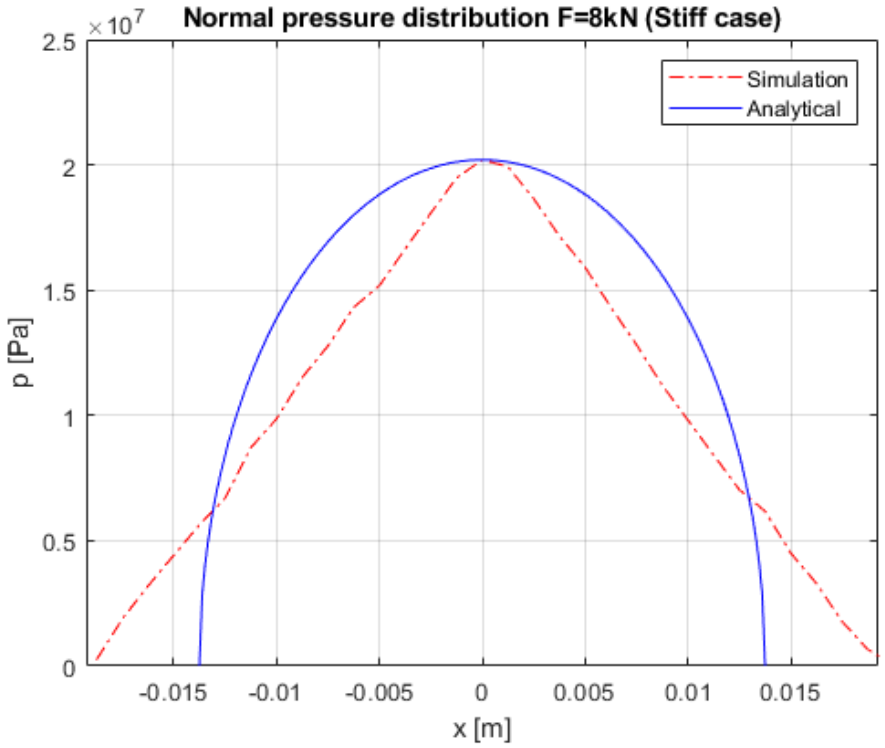

Figure B.16: Pressure distribution - $Fn = 8$kN (stiff case)

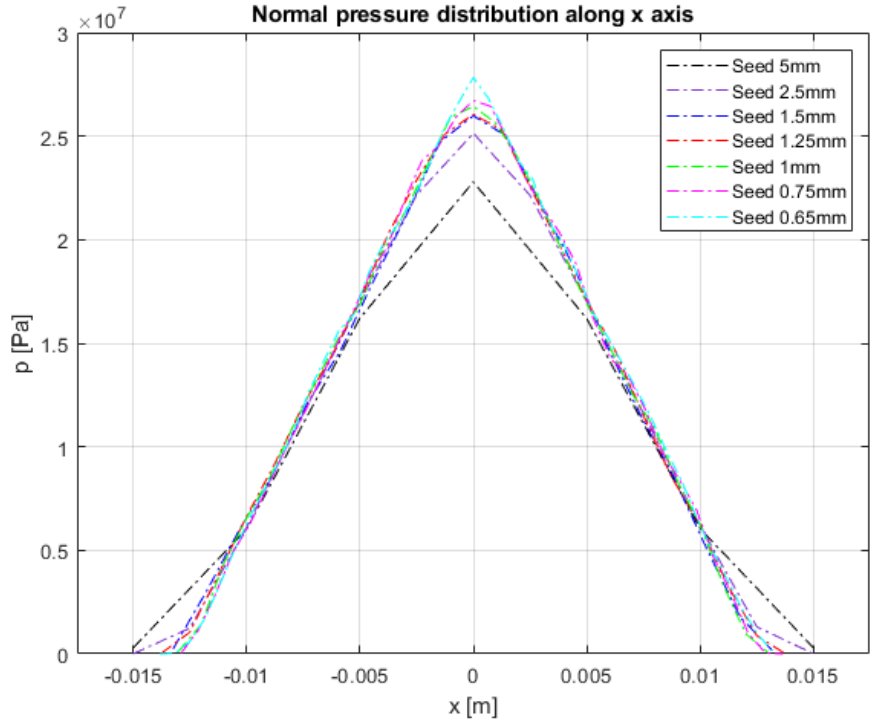

Figure B.17: Pressure distribution - mesh convergence study (stiff case)

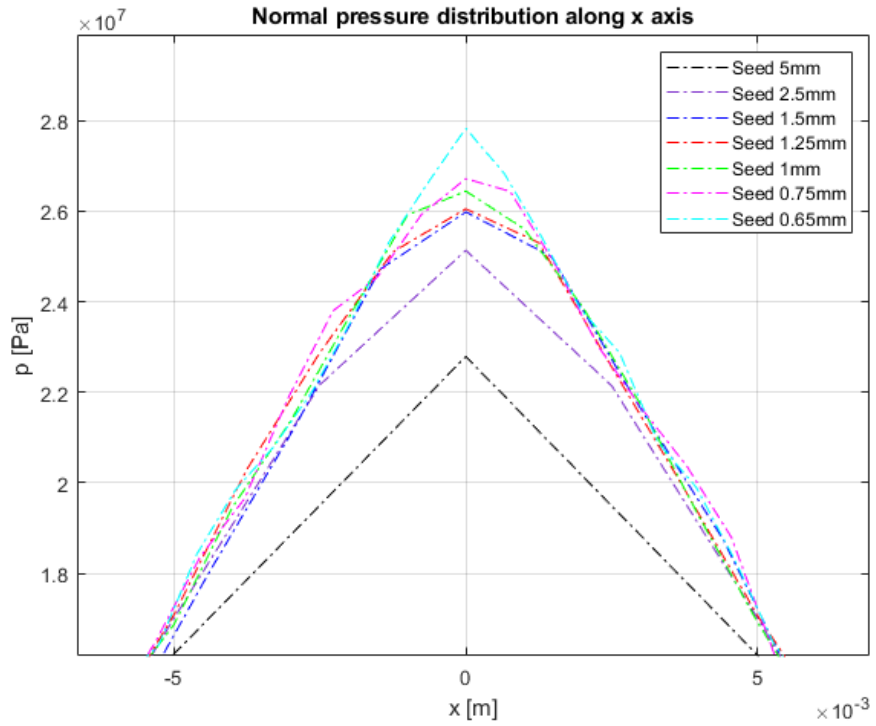

Figure B.18: Pressure distribution zoomed - mesh convergence study (stiff case)

C

Appendix C

This appendix contains additional results of simulations using the worn pole shoe.

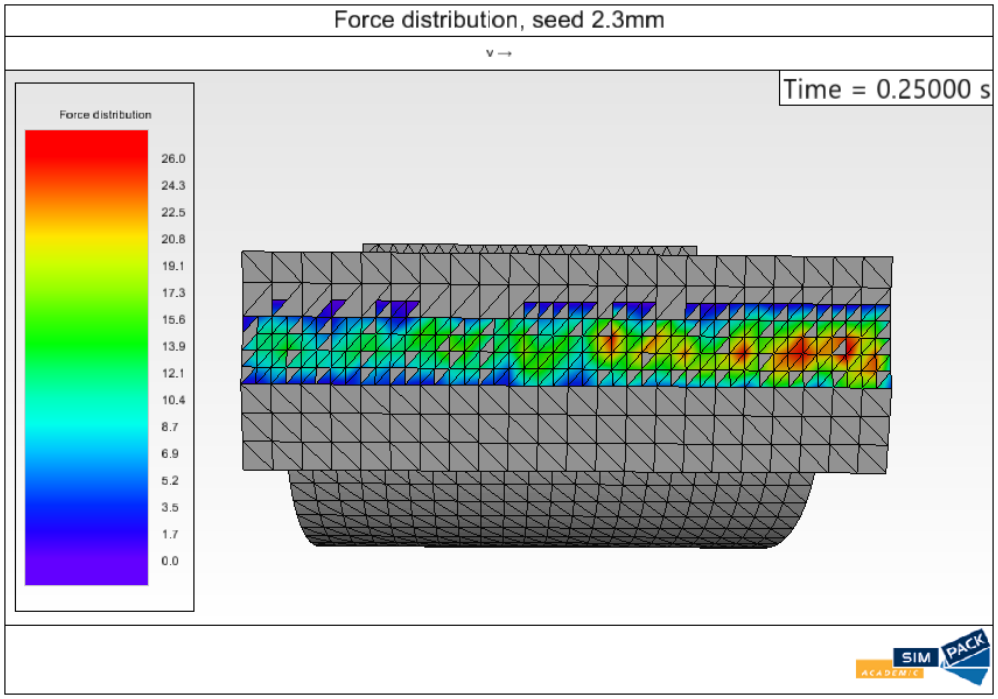

Figure C.1: Force distribution on the pole shoe, seed 2.3mm

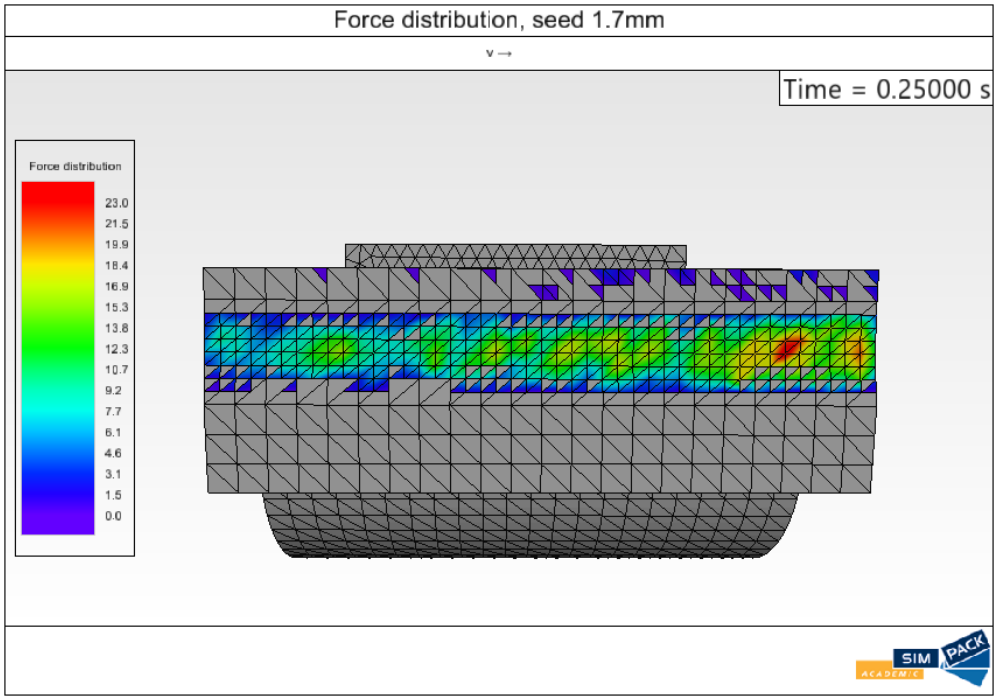

Figure C.2: Force distribution on the pole shoe, seed 1.7mm

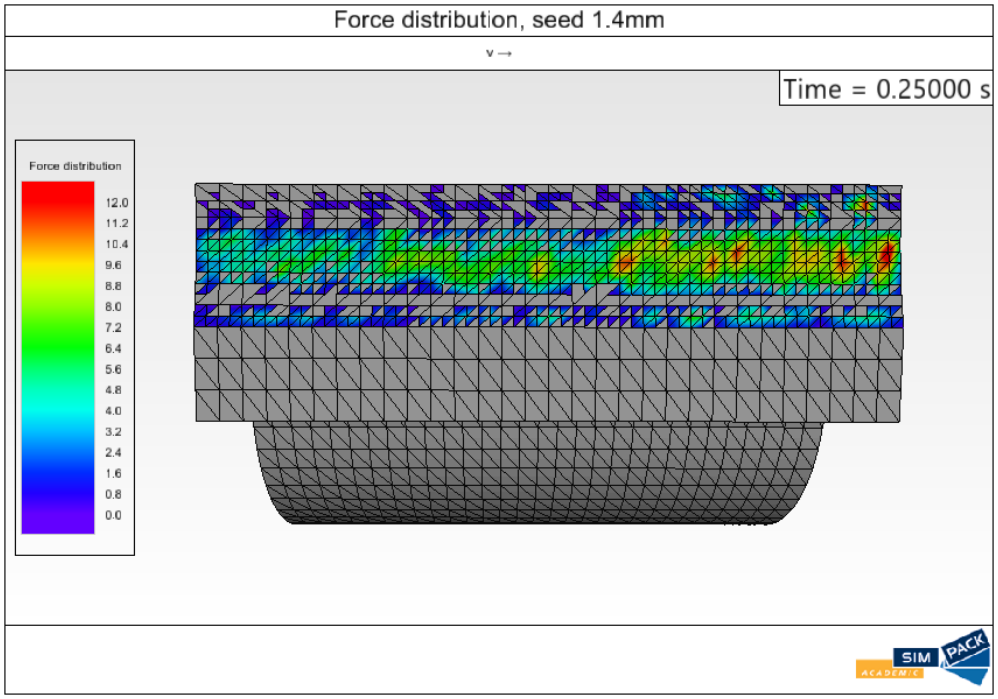

Figure C.3: Force distribution on the pole shoe, seed 1.4mm

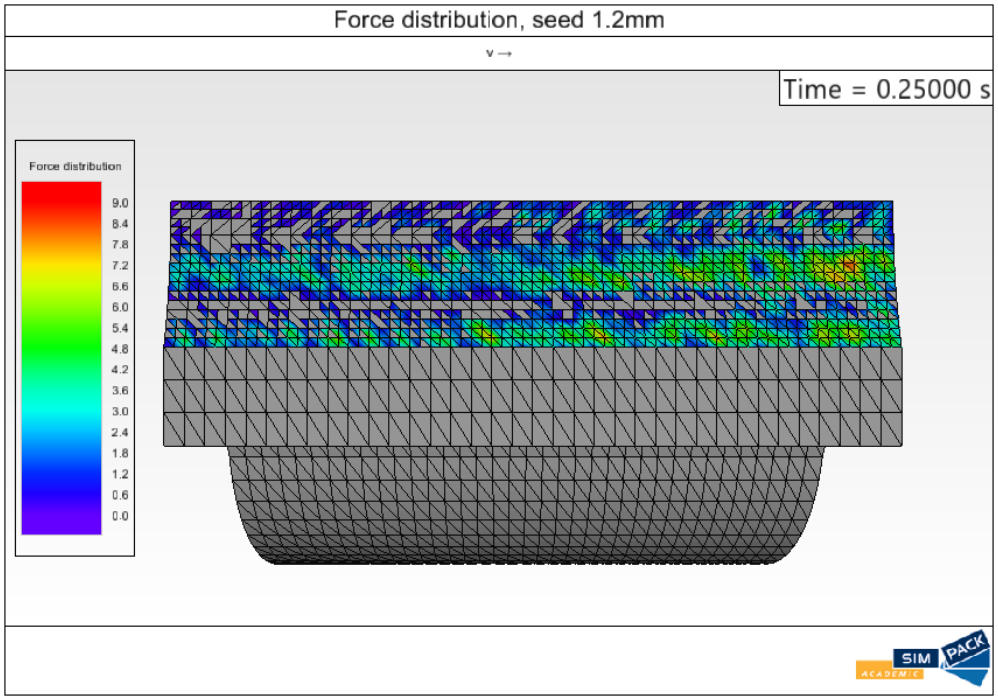

Figure C.4: Force distribution on the pole shoe, seed 1.2mm

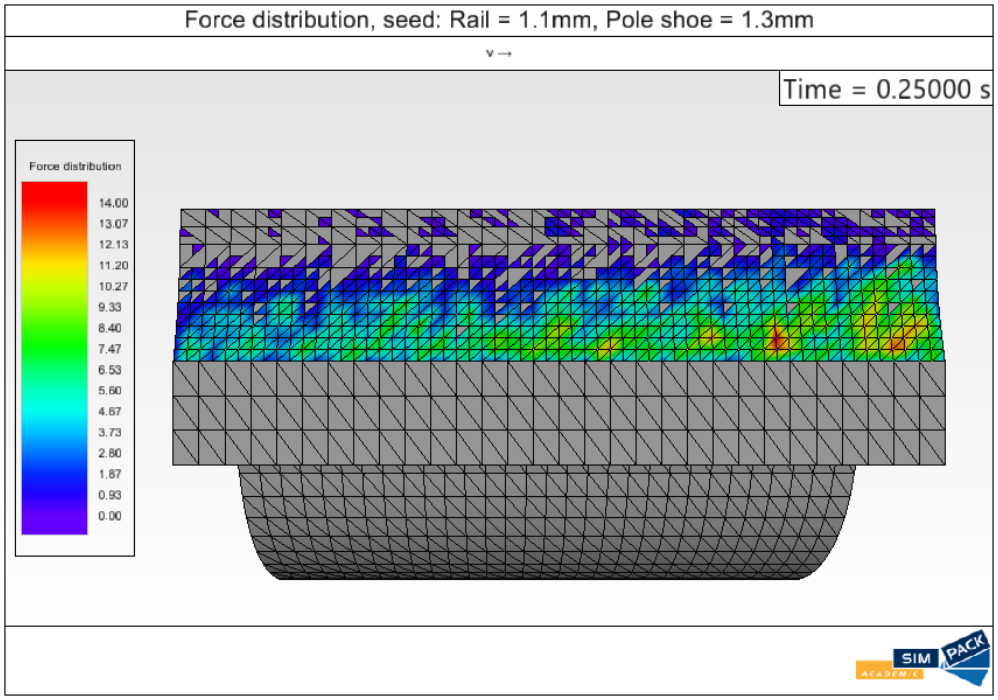

Figure C.5: Force distribution on the pole shoe, seed: Rail = 1.1mm, Pole shoe = 1.3mm

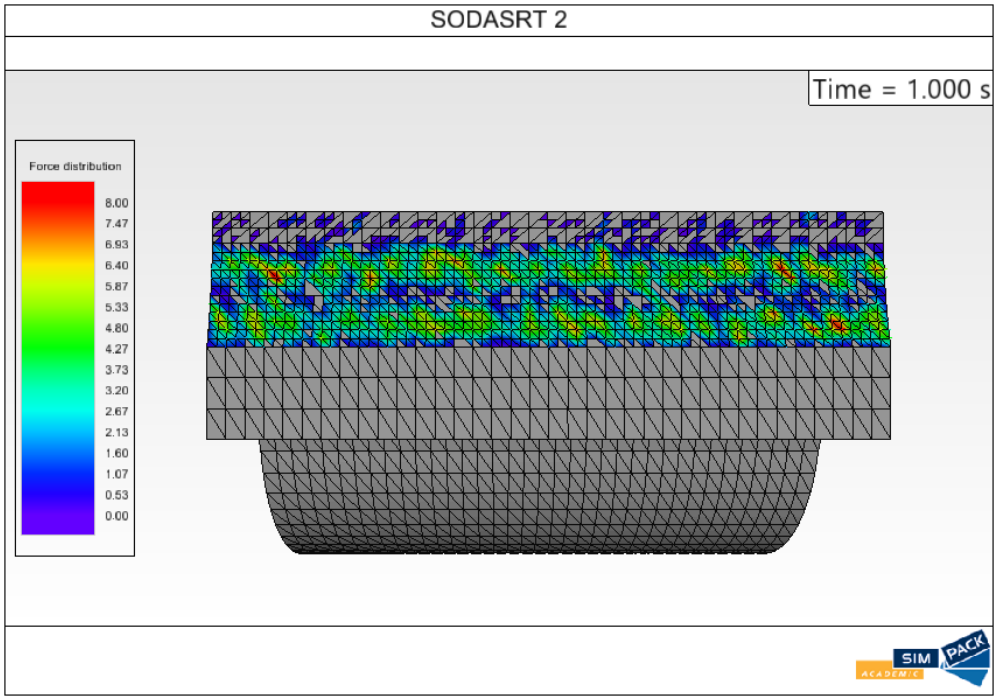

Figure C.6: Force distribution on the pole shoe, Solver SODASRT2

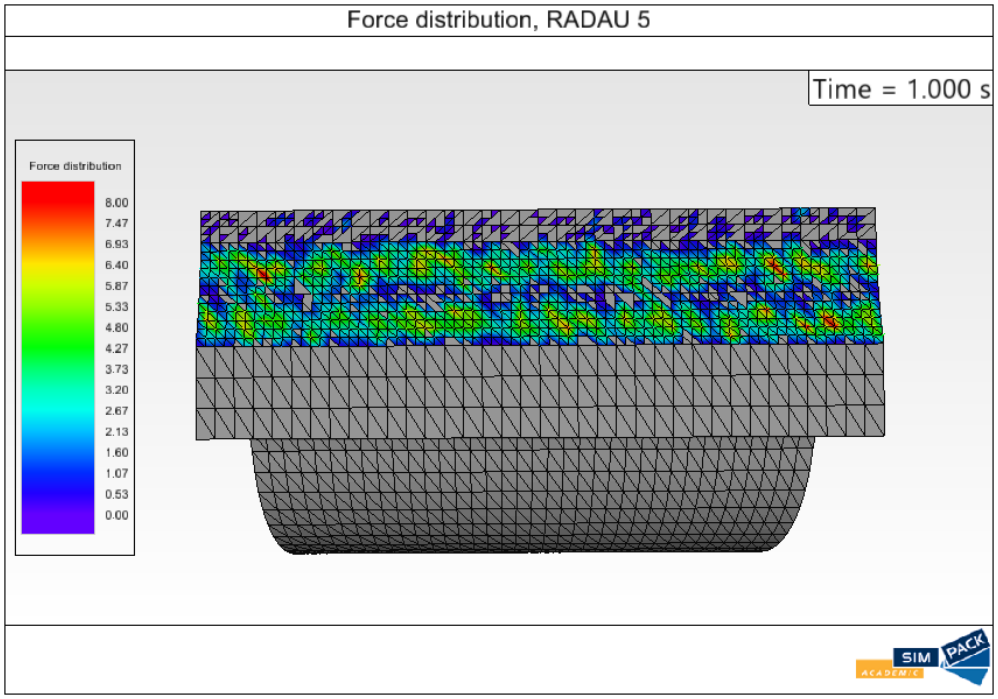

Figure C.7: Force distribution on the pole shoe, Solver RADAU5

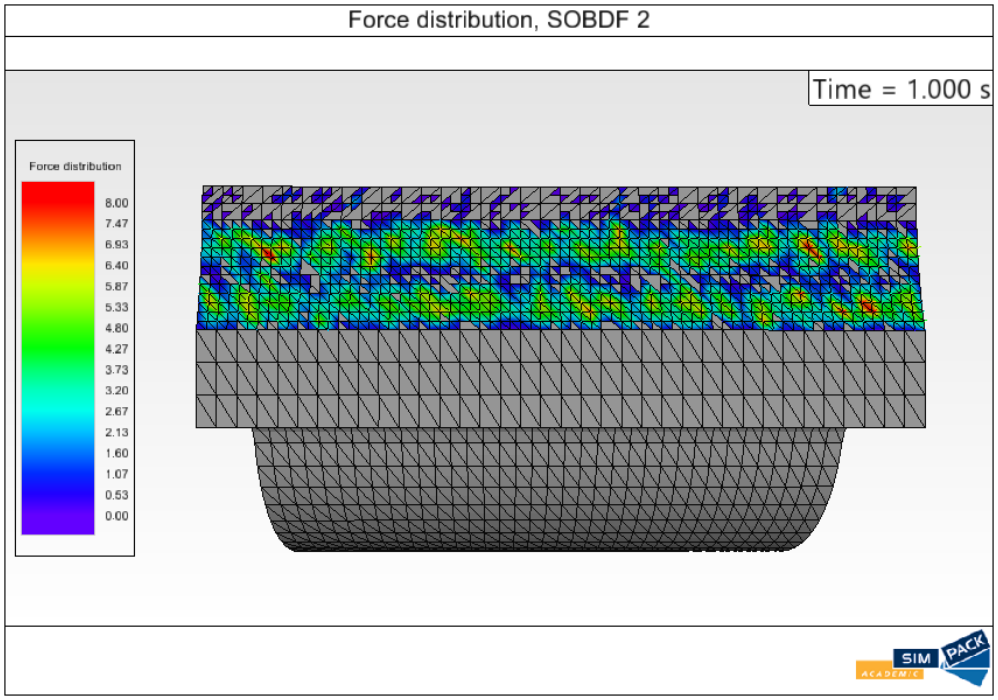

Figure C.8: Force distribution on the pole shoe, Solver SOBDF 2

DEPARTMENT OF MECHANICS AND MARITIME SCIENCES
CHALMERS UNIVERSITY OF TECHNOLOGY
Gothenburg, Sweden 2025
www.chalmers.se

CHALMERS
UNIVERSITY OF TECHNOLOGY